

# Abnormalities in the Motor Unit of a Fast-Twitch Lower Limb Skeletal Muscle in Huntington's Disease

ASN Neuro  
Volume 11: 1–20  
© The Author(s) 2019  
Article reuse guidelines:  
sagepub.com/journals-permissions  
DOI: 10.1177/1759091419886212  
journals.sagepub.com/home/asn



Priscila Aparecida Costa Valadão<sup>1</sup>, Bárbara Campos de Aragão<sup>1</sup>,  
Jéssica Neves Andrade<sup>1</sup>, Matheus Proença S. Magalhães-Gomes<sup>1</sup>,  
Giselle Foureaux<sup>1</sup>, Julliane Vasconcelos Joviano-Santos<sup>1</sup>,  
José Carlos Nogueira<sup>1</sup>, Thatiane Cristina Gonçalves Machado<sup>1</sup>,  
Itamar Couto Guedes de Jesus<sup>2</sup>, Julia Meireles Nogueira<sup>1</sup>,  
Rayan Silva de Paula<sup>1</sup>, Luisa Peixoto<sup>1</sup>, Fabíola Mara Ribeiro<sup>3</sup> ,  
Juan Carlos Tapia<sup>4</sup>, ÉriKa Cristina Jorge<sup>1</sup>, Silvia Guatimosim<sup>2</sup>, and  
Cristina Guatimosim<sup>1</sup> 

## Abstract

Huntington's disease (HD) is a disorder characterized by chronic involuntary movements, dementia, and psychiatric symptoms. It is caused by a mutation in the gene that encodes for huntingtin protein (HTT), leading to the formation of mutant proteins expressed in various tissues. Although brain pathology has become the hallmark for HD, recent studies suggest that damage of peripheral structures also contributes to HD progression. We previously identified severe alterations in the motor units that innervate cervical muscles in 12-month-old BACHD (Bacterial Artificial Chromosome Huntington's Disease) mice, a well-established mouse model for HD. Here, we studied lumbar motoneurons and their projections onto hind limb fast-twitch skeletal muscles (tibialis anterior), which control balance and gait in HD patients. We found that lumbar motoneurons were altered in the HD mouse model; the number and size of lumbar motoneurons were reduced in BACHD. Structural alterations were also present in the sciatic nerve and neuromuscular junctions. Acetylcholine receptors were organized in several small patches (acetylcholine receptor fragmentation), many of which were partially innervated. In BACHD mice, we observed atrophy of tibialis anterior muscles, decreased expression of glycolytic fast Type IIB fibers, and at the ultrastructural level, alterations of sarcomeres and mitochondria. Corroborating all these findings, BACHD animals performed worse on motor behavior tests. Our results provide additional evidences that nerve–muscle communication is impaired in HD and that motoneurons from distinct spinal cord locations are similarly affected in the disease.

## Keywords

BACHD mice, lumbar spinal cord, motoneurons, tibialis anterior

Received July 4, 2019; Revised August 8, 2019; Accepted for publication August 17, 2019

## Introduction

Skeletal muscle loss and dysfunction are found in Huntington's disease (HD), which is a progressive neurodegenerative disorder caused by an autosomal dominant condition leading to motor, cognitive, and psychiatric impairment. In 1993, the Huntington's Disease Collaborative Research Group identified a mutation in the short arm of Chromosome 4, an unstable

<sup>1</sup>Departamento de Morfologia, Universidade Federal de Minas Gerais, Belo Horizonte, Brazil

<sup>2</sup>Departamento de Fisiologia e Biofísica, Universidade Federal de Minas Gerais, Belo Horizonte, Brazil

<sup>3</sup>Departamento de Bioquímica e Imunologia, Universidade Federal de Minas Gerais, Belo Horizonte, Brazil

<sup>4</sup>Department of Biomedical Sciences, University of Talca, Chile

### Corresponding Author:

Cristina Guatimosim, Departamento de Morfologia, Instituto de Ciências Biológicas, Universidade Federal de Minas Gerais, Av. Antônio Carlos, 6627, Belo Horizonte, Minas Gerais 31270-901, Brazil.

Email: cguati@icb.ufmg.br



expansion in the number of CAG repeats in the huntingtin (HTT) protein (MacDonald et al., 1993). Historically, HD has been studied in the central nervous system (CNS), mainly in neurons from the basal ganglia and cerebral cortex (Reiner et al., 1988; Novak and Tabrizi, 2010; Reinius et al., 2015).

The discovery of HTT gene mutation opened a new scenario for scientific research enabling the generation of numerous animal models for the disease (L. B. Menalled and Chesselet, 2002; Heng et al., 2008; L. Menalled et al., 2009; Yang and Gray, 2011). Experiments performed in these animal models allowed the identification of mutant huntingtin protein (mHTT) not only in the CNS but also in peripheral structures, such as skeletal muscles (van der Burg et al., 2009; Zielonka et al., 2014; Mielcarek et al., 2017). In fact, mouse HD models exhibited pronounced skeletal muscle atrophy, a pathophysiological finding that could be due to accumulation of mHTT in skeletal muscles, motoneurons, or both (Khedraki et al., 2017). This prompted the question of whether a primary defect in the neuromuscular system contributes to the motor deterioration observed in patients with HD, independently of the striatal degeneration (van der Burg et al., 2009). Consistent with this hypothesis, Ribchester et al. (2004), using the R6/2 mouse model, identified physiological and morphological alterations on neuromuscular junctions (NMJs), a result that suggested a progressive disruption of the communication between motoneurons and skeletal muscles. However, it is important to note that these authors did not investigate whether there is denervation in the NMJs of R6/2 mice.

Recently, using a different mouse model for HD (BACHD), which expresses the full-length human mHTT in a Bacterial Artificial Chromosome vector, we reported alterations in cervical motor units (MUs), such as the reduction in the number and size of motoneurons, axonal degeneration, and fragmentation of NMJs. Furthermore, marked muscle atrophy and fiber-type switching were observed in BACHD-sternomastoid (STM) muscles (Valadão et al., 2017). In addition, we also described abnormal NMJs in the diaphragm of BACHD mice (Valadão et al., 2018). Nonetheless, the hypothesis that HD may have a more direct connection with progressive disruption of communication between motoneurons and skeletal muscles remains poorly explored.

Following the trail initiated in our previous studies, we investigated whether mHTT-mediated alterations were restricted to cervical motoneurons or spread over other spinal cord segments like the lumbar segment. This comparison has clinical importance, because in amyotrophic lateral sclerosis, which is a disease that affects the motoneurons, there are evidences that upper and lower motor neurons are differently affected during the course of the disease (Eisen et al., 1992; Fischer et al., 2004, reviewed

by Van den Bos et al., 2019). Thus, studying two different segments of the spinal cord in the BACHD animal model, which shows clear loss of motoneurons, is an important study in the sense of identifying possible differences in these two regions (cervical and lumbar segments) in this HD model. To this end, we chose to look at the lumbar spinal cord segment and the MU of the lower hind limb muscle tibialis anterior (TA). This muscle controls movement and balance that are severely impaired in HD such as decreased walking speed, difficulties in starting the steps, and variable pattern of step. In addition, motor neurons of the lumbar spinal cord segment and TA muscle are also involved in gait, which is considered to be one of the main factors of disability in patients with HD (Piira et al., 2013). It is noteworthy that, with the progression of the disease, the mobility is affected, increasing the risk of falls and directly impacting the functionality of the patients who end up needing constant help in their daily living activities (Koller and Trimble, 1985; Thaut et al., 1999; Wheelock et al., 2003; Bilney et al., 2005; Carroll et al., 2015; T. M. Cruickshank et al., 2015).

In this way, this study adds to our previous work, because the focus now is to examine another segment of the spinal cord, with motoneurons that are involved in the innervation of muscle groups with function (TA is dorsiflexion and inversion of the foot) and composition (predominantly a fast contraction muscle) different from the STM muscle previously studied by us.

## Materials and Methods

### BACHD Mice

All experiments were performed according to the rules established by the local animal care committee (Ethics Committee on Animal Experiments of the Universidade Federal de Minas Gerais (UFMG)); approved protocol #036/2013. All efforts were made to minimize animal suffering and to reduce the number of animals used. This study was not preregistered.

The FVB/NJ (wild type [WT]) and FVB/N-Tg (HTT\*97Q)IXwy/J (BACHD) transgenic mice (male) were purchased from Jackson Laboratory (Bar Harbor, ME, USA; JAX stock #008197) and used to establish a new colony. Mice were held in a place with controlled temperature (23°C) in a 12–12 hr light–dark cycle. Food and water were provided *ad libitum* in an animal care facility of the Department of Physiology and Biophysics, UFMG. All animals used in this study were genotyped 10 days after birth using multiplex polymerase chain reaction (PCR; HTT-forward: CCGCTCAGGTTCTGCTTTTA/HTT-reverse: GGTCGGTGCAGCGGCTCCTC; actin-forward: TGGAATCGTGTGGC

ATCCATCA/actin-reverse: AATGCCTGGGTACATG GGGTA).

The BACHD mouse model, unlike the R6/2 model, expresses the total length of human mHTT inserted into the Bacterial Artificial Chromosome (Gray et al., 2018). Compared with the R6/2 model, BACHD has an expressive vantage, because in addition to presenting behavioral and pathological characteristics of the disease, it also has the polyglutamine sequence *CAA/CAG* in a more stable form, thus the length of the *CAA/CAG* repeat in BACHD mice is stable in 97 replicates over several generations (Yang et al., 1997). In this way, this model is reliability for the study of long-term phenotypic characteristics as we did in 12-month-old animals (Yang et al., 1997; Kazantsev et al., 1999). In addition to these characteristics, this model has a normal life span with slow disease progression, allowing more detailed longitudinal studies when compared with other rapid progression models, such as R6/2, for example (Yang and Gray, 2011).

Animals were identified by numbers according to their genotype (WT or BACHD). They were separated into mini-isolator cages with a maximum of four animals per cage. In this study, we used WT and BACHD mice (weight average for WT = 27.55 g and BACHD = 41.06 g). Using a table of random numbers, animals were randomly divided into two groups. Our experiments were performed on 12-month-old WT and BACHD animals, as previous studies using this model demonstrated pronounced neurodegeneration in the cerebral cortex and deficits in motor behavior in mice of this age (Gray et al., 2008; for review, see Yang and Gray, 2011). Also, this age corresponds to middle age in humans, when it is supposed to appear HD symptoms. In addition, previous work from our research group have shown that 12-month-old BACHD mice present alterations in cardiac cells and other muscles such as STM and diaphragm (Valadão et al., 2017, 2018; Joviano-Santos et al., 2019).

For all experiments involving morphology and immunofluorescence techniques, mice from both genotypes (WT and BACHD) were deeply anesthetized with ketamine/xylazine (0.1 mL/20 g) in accordance with the Ethics Committee on Animal Experiments of the UFMG protocol. All surgical procedures were described in the appropriated sections. The experimental procedures were performed in the afternoon and, by the end of each surgical procedure, the animals were euthanized by an overdose of anesthetics.

The experimental procedures were performed in the Departments of Morphology and Pharmacology at the UFMG. The experimental groups remained constant from the beginning to the end of the study, and the exact numbers for all experiments are provided in the figure captions/“Results” section.

## Lumbar Spinal Cord Immunofluorescence

All immunofluorescence experiments were performed according to the protocol described by Valadão et al. (2017). For the identification of alpha-motoneurons, lumbar spinal cords slices were stained with choline acetyltransferase (ChAT) antibody (1:100, Cat #AB1582 RRID: AB\_11211009) and with osteopontin (OPN; 1:100, R&D Systems Cat #MAB14331 RRID: AB\_2194980). Lumbar spinal cords (L1–L5 segments) were removed and fixed with 4% paraformaldehyde (PFA) for 48 hr. Next, the spinal cord segments were kept in 30% sucrose for 24 hr. Samples were then frozen in isopentane (Sigma-Aldrich), cooled with liquid nitrogen, and stored at  $-80^{\circ}\text{C}$ . The lumbar spinal cords cross-sections (30  $\mu\text{m}$ ) were cut on a cryostat (Leica CM3050S) and collected on gelatin-coated slides. The sections were blocked (60 min, room temperature [RT]) in solution containing 3% bovine serum albumin (BSA), 5% donkey serum, and 0.1% Triton X-100. Samples were then incubated overnight at  $4^{\circ}\text{C}$  with the following primary antibodies diluted in 3% BSA, 5% donkey serum, 5% goat serum: goat anti-ChAT and mouse anti-OPN. Slides were washed 3 times with phosphate-buffered saline (PBS)  $1\times$ , and incubated for 2 hr at RT with the secondary antibodies Alexa 488 donkey antigoat IgG1 for anti-CHAT (1:800, Molecular Probes Cat.#A-11055 RRID: AB\_142672) and Alexa 488 goat antimouse for anti-OPN (1:1,000; Thermo Fisher Scientific Cat. #A-21042 RRID: AB\_2535711). Samples were washed 3 times with PBS  $1\times$  and mounted using ProLong<sup>®</sup> Gold antifade (Thermo Scientific Invitrogen<sup>™</sup>). Images were acquired using a  $63\times$  oil immersion (numerical aperture [NA] 1.4) objective attached to a laser-scanning confocal microscope (Zeiss LSM 510 Meta; Zeiss GmbH, Jena, Germany). An Argon (488 nm) laser was used for excitation of lumbar spinal cord slides marked with anti-ChAT and anti-OPN. The Z series of optical sections were collected at 2.0  $\mu\text{m}$  intervals. All digital images were quantitatively analyzed using Image J software (Wayne Rasband, National Institutes of Health [NIH], USA).

Caspase-3 staining in BACHD mice spinal cords lumbar segments (L1–L5) was performed by immersing the spinal cord in neutral-buffered formalin for 24 hr. The samples were then dehydrated in ethanol (70%, 80%, 90%, 95%, and 100%), cleared in xylene, embedded in paraffin, and cut (thin sections—5  $\mu\text{m}$ ) using a microtome (model HM335E; Microm, Inc., Minneapolis, MN, USA). Nonspecific blockade was performed by incubation of the samples in a solution containing 2% BSA, 0.1% Tween-20 for 1 hr in a moist chamber. Samples were incubated with the primary antibody (1:100 polyclonal rabbit anticaspase-3;

Sigma-Aldrich, Saint Louis, MO, USA) diluted in blocking solution (overnight at 4°C in a moist chamber) and then washed 3 times with PBS following incubation with the secondary antibody (1:1,000, Alexa Fluor 488 goat antirabbit; Invitrogen, Eugene, OR, USA) for 1 hr. To allow nuclei identification, sections were washed 3 times with PBS and stained with 4',6-diamidino-2-phenylindole (1:1,000; Invitrogen). The stained sections were imaged using a NIKON ECLIPSE Ti microscope (100× objective, NA: 1.49). All digital images were quantitatively analyzed using Image J software (Wayne Rasband, NIH, USA).

To perform the counting of motoneurons marked with CHAT, OPN, and caspase-3, only those with evident nuclei were measured. As the motoneurons are variable and not perfect circles, we chose to use the *Feret diameter* present in the Image J software (Feret diameter) to measure the diameter of these cells. This tool uses mathematical calculations to correct the diameter of figures that are not totally spherical. In general, it can be defined as the common base of a group of diameters derived from the distance of two tangents to the particle contour in a well-defined orientation (Yap et al., 2013).

### NMJ Immunofluorescence and Confocal Microscopy Analysis

Six mice were anesthetized (three per genotype) as previously described with ketamine/xylazine (0.1 mL/20 g) and transcardially perfused with ice-cold 4% PFA in 0.1M PBS (PBS; pH 7.4). The TA muscles were dissected, blocked in 3% BSA + 5% goat serum + 0.5% Triton X-100 for 30 min at RT, and stained with antisynaptotagmin antibody (1:250, antisynaptotagmin, antimouse, IgG2A, Developmental Studies Hybridoma Bank [DSHB]; Cat #3H2 2D7 RRID: AB\_528483) in the blocking solution. The samples were then incubated overnight at 4°C, washed 3 times with PBS, and incubated for 1 hr at RT with Alexa 555- $\alpha$ -bungarotoxin ( $\alpha$ -btx; 1:1,000; Cat# T1175 Molecular Probes; Invitrogen; T1175 RRID: AB\_2313931) together with secondary antibody (1:1,000, Alexa-488 goat antimouse IgG2A; Invitrogen; Cat #A-21141 also A21141 RRID: AB\_141626). The muscles were washed 3 times with PBS and whole-mounted using Vectashield (Vector Laboratories, Eching, Germany). Images of NMJs were acquired using a 63× oil immersion (NA: 1.4) objective attached to a laser-scanning confocal microscope (Zeiss LSM 510 Meta; Zeiss GmbH, Jena, Germany). We used an argon (488 nm) and helium–neon (He–Ne, 543 nm) lasers to excite the samples. The Z series optical sections were collected at 2.0  $\mu$ m intervals, and the whole TA muscle samples were scanned. The nerve terminals were identified considering their colocalization near the acetylcholine receptor (AChR) clusters. Images were converted

to a grayscale format (eight bits), and each synaptic element was individually evaluated. The fragmentation index of the NMJs was obtained using the particles analysis method described in Valadão et al. (2017). Briefly, the images were converted into a binary image pattern and were skeletonized. Next, to describe the connectivity for each pixel in the image, a histogram was generated using the BinaryConnectivityClass plugin from ImageJ (Pratt et al., 2013). We analyzed the degree of fragmentation in pre- and postsynaptic elements comparing the muscle samples from WT and BACHD mice. The parameters adopted for fragmentation were defined according to the evaluation criteria described by Valdez et al. (2010), which establishes fragmentation by five or more islands both in the presynaptic and postsynaptic membranes. We analyzed 50 NMJs for each animal.

### Gene Expression Analysis

The TA muscles of five WT and five BACHD mice were frozen in nitrogen, macerated, and added to 1 mL of TRI Reagent (Sigma) for total RNA extraction. Posteriorly, 1  $\mu$ g of RNA was used, following manufacturer's recommendations, for cDNA synthesis using the M-MLV Reverse Transcriptase Kit (Invitrogen). To check for changes in muscle gene expression that are characteristic of denervation, we studied the expression level of several genes known to change during denervation. Measurement of mRNA levels was performed by quantitative PCR containing 5  $\mu$ L of iTaq™ Universal SYBR Green Supermix (Bio-Rad), 0.4  $\mu$ M of each of the primers, 1  $\mu$ L cDNA diluted 1:10 in water and final volume adjustment to 10  $\mu$ L with nuclease-free water. Reactions occurred at 50°C for 2 min, 95°C for 2 min, and 40 cycles of 94°C for 15 s, 60°C for 15 s, and 72°C for 20 s in the Rotor Gene™ 3000 machine. Target genes (Table S1) tested in this work were as follows: Cholinergic Receptor Nicotinic Alpha 1 Subunit (*Chrna1*), Cholinergic Receptor Nicotinic Gamma Subunit (*Chrng*), Growth Differentiation Factor 5 (*Gdf5*), and RUNX Family Transcription Factor 1 (*Runx1*). Gene expression was normalized to the geometric mean of the following selected reference genes: Actin Beta (ACTB) and Ribosomal Protein L39 (Rpl39).

### Western Blot

To detect synaptotagmin protein in TA muscle nerve endings, 50 mg protein were separated by SDS-PAGE. The antibody used and its sources are follows: antisynaptotagmin, antimouse, IgG2A, DSHB, 1: 2,000; Cat # 3H2 2D7 RRID: AB\_528483. The validation data for each antibody were obtained from the data sheet provided by the company. For immunodetection, we use improved chemiluminescence (Amersham Biosciences).

Protein levels were expressed as a ratio of optical densities. Glyceraldehyde 3-phosphate dehydrogenase was used as a protein loading control.

### **Morphology and Morphometric Analysis of Sciatic Nerve and TA Muscle Fibers**

The TA muscle was dissected-out and fixed in 4% glutaraldehyde diluted in PBS (0.2M) for 24 hr at RT. After dehydration in an ascending series of alcohols (70%, 80%, 90%, 95% 2×), samples were embedded in glycolmethacrylate resin (Leica) and sectioned (5 μm) in a microtome (Reichert Jung). Sections from the TA muscle were stained with toluidine blue Electron Microscopy Sciences(EMS), and the cross-sectional area (CSA) of individual myofibers imaged using a light microscope (10× oil objective-Leica DM2500) coupled to a charge-coupled device (CCD) camera (Leica DFC345FX).

Samples containing the sciatic nerve were histologically analyzed. Semi-thin cross-sections (300 nm) were obtained and stained with toluidine blue. Images of whole sciatic nerve cross-sections from WT and BACHD mice were captured using a 20× objective in a ZEISS Axio Lab.A1 microscope. The total CSA of the nerve was measured using ImageJ plugins (NIH), and the total number of axons was counted. Like the motoneurons, the axons are not perfect circles and we also used the Feret diameter (described earlier) for the calculation of the total diameter (axon diameter). To quantify axonal myelination, we used the *G* ratio, which was calculated measuring the axonal inner diameter and dividing it by the outer diameter following the formula:  $G = d/D$ , where *G* is the *G* ratio, *d* is the inner diameter, and *D* is the outer diameter (Chau et al., 2000).

### **TA Muscle Fiber Typing**

TA muscle fiber typing was performed according to the protocol described by Valdez et al. (2012). TA samples were put in freezing molds covered with *optimum cutting temperature* freezing medium (Easy Path), and fresh frozen in isopentane (Sigma-Aldrich) cooled with liquid nitrogen and stored at −80°C. The mid-belly region of the TA muscle was cut on a cryostat (Leica CM3050S), and the cross-sections (10 μm) collected on gelatin-coated slides. Slides containing muscle sections were then blocked for 30 min at RT with 3% BSA (Sigma-Aldrich), 5% goat serum (Sigma-Aldrich), and 0.1% Triton X-100 (Sigma-Aldrich) diluted in PBS 1×. Muscle sections were incubated overnight at 4°C with the following primary antibodies: Type 1 (1:250, Leica Microsystems Cat# NCL-MHCs RRID: AB\_563898), Type 2A (1:100, DSHB Cat# SC-71 RRID: AB\_2147165), Type 2X (1:100, DSHB Cat# BF-35

RRID:AB\_2274680, which recognizes all types of muscles fibers except 2X), and Type 2B (1:100, DSHB Cat# BF-F3 RRID:AB\_2266724). All antibodies were diluted in 3% BSA, 5% goat serum prepared in PBS 1×. Slides were washed 3 times with PBS 1× and incubated for 1 hr at RT with secondary antibodies Alexa 488 goat antimouse IgG1 (Thermo Fisher Scientific Cat # A-21121 RRID: AB\_2535764; it recognizes Type 1, Type 2A, and Type 2X antibodies) and Alexa 488 goat antimouse IgM (Thermo Fisher Scientific Cat #A-21042 RRID: AB\_2535711 It recognizes Type 2B antibody). The samples were washed 3 times with PBS 1× and mounted using VectaShield antifade solution (Vector Laboratories Cat #H-1000 RRID: AB\_2336789). Images were acquired using an air objective (10×, 0.25 NA) in an epi-fluorescence microscope (Leica DM2500) equipped with a Leica DFC345FX camera and visualized in a computer. The excitation light came from a 100 W Hg lamp, and an fluorescein isothiocyanate (FITC) filter cube was used to collect the emitted light. Whole muscle cross-sections were imaged for analysis. Each fiber type was expressed as a percentage of the total number of fibers. Validation for each antibody was obtained from the datasheets provided by the company. The CSA of individual myofibers from each fiber type was measured.

### **Transmission Electron Microscopy**

For the ultrastructural studies, we used the protocol previously described by us (Rodrigues et al., 2013). Briefly, mice were anesthetized with ketamine/xylazine (0.1 mL/20 g), and the heart left ventricle perfused with ice-cold modified Karnovsky fixative (4% PFA and 2.5% glutaraldehyde in 0.1M sodium cacodylate buffer at 4°C) and maintained in the solution for at least 24 hr at 4°C. Lumbar spinal cord segments (L1–L5) and TA muscles from WT and BACHD transgenic mice were then collected. After fixation, samples were washed with cacodylate buffer (0.1M), cut into several fragments (300 nm), postfixed in reduced osmium (1% osmium tetroxide containing 1.6% potassium ferrocyanide), contrasted *en bloc* with uranyl acetate (2% in deionized water), dehydrated through an ascending series of ethanol solutions, and embedded in EPON (epoxy resin). After several days in the oven at 60°C, the resin blocks were sectioned (50 nm), and the ultra-thin sections collected on 200 or 300 mesh copper grids and contrasted with lead citrate. The ultra-thin sections were viewed with a Tecnai-G2-Spirit FEI/Quanta electron microscope (120 kV Philips).

To quantify the lipofuscin granules in the motoneurons, we used 30 electron micrographs of the lumbar spinal cord motoneurons for each genotype (WT, BACHD). The counting was performed using the ImageJ software plugins (NIH). Data were presented as granules/area using the GraphPad Prism 6.

### Motor Behavioral Tests

We used the test paw print test to examine the pattern of steps of mice hind limbs during the locomotion (adapted from de Lagrán et al., 2004). Briefly, the apparatus consisted of a narrow wooden tunnel ( $10 \times 10 \times 70$  cm), lined with white paper, containing a dark box at one of its ends (positive reinforcement) and positioned in an illuminated room (aversive stimulus). Rodents naturally seek to be lodged in safer and dimly lit environments, so when the animal were placed at the end of the corridor opposite the box, they naturally tended to walk toward it. The hind legs of the animals were previously painted with nontoxic black ink, so that when walking on paper, the footprints of their legs were printed/recorded. This procedure was repeated at least 3 times (three trials) for each animal.

The gait pattern of each animal was recorded through four gait cycles for each trial and data were expressed as the mean of at least three trials. A complete gait cycle was previously defined by de Lagrán et al. (2004), as the distance from one pair of hind legs to the next pair of hind legs. Three parameters were evaluated: the length and the width of the step and the size of the step (right and left). The length of the pitch was measured as the average distance of locomotion between one leg and the next immediately ahead. The width was measured as the mean distance between the right and left hind legs. The length of the stride was considered as the distance between each cycle (right and left). These variables were expressed in centimeters.

The data obtained through the behavioral tests were plotted in Microsoft Excel<sup>®</sup> and converted to graphical representations through the program GraphPad Prism 7.0 (San Diego, CA, USA).

Spontaneous locomotor activity was evaluated by means of an automatic open field (LE 8811 IR Motor Activity Monitors Panlab/Harvard Apparatus), with acrylic box dimensions  $450 \times 450 \times 200$  mm (width  $\times$  depth  $\times$  height; Pereira et al., 2014). The WT and BACHD animals were habituated in the behavioral testing room for the minimum time of 60 min. The activities detected in the horizontal plane (distance traveled and mean velocity) were measured for 60 min. The measure of activity total was calculated using the ACTITRACK program, and the statistical analyses were performed using GraphPad Prism 6 software.

The wire hang test is a measure of the force muscle (fore and hind limbs) analysis in rodents, and the experiments were conducted according to protocol described by Sango et al. (1996) and Prado et al. (2006). The animals were accustomed to the experimental room and manipulated by the researcher at least 2 hr before of the test. The apparatus used consisted of a metal grid with spacing of 1 cm between the 0.8 mm diameter bars. The test was

conducted in a single session in which the animal was individually placed on the grid until the hold. The grid was then inverted and maintained at 20 cm above a foam. It is important to note that this height is sufficient for the animal to remain attached to the grid; however, it is unable to injure it in the event of fall. The latency, which is the time until the animal disengaged and fell off the inverted grid for 60 s observation, was measured, and three observations per animal were considered. It is important to emphasize that we use time/weight (time corrected for weight), because the BACHD mice presented weight gain, and for this reason, we corrected the time spent in the apparatus by the weight of the animal. The time was counted in seconds and the weight in grams.

The grip strength test was performed according to Fowler et al. (2002). To this end, the power transducer was connected to a small metal bracket that could be grasped by the mouse. The force transducer was coupled to a computer that recorded the maximum grip force in fore limbs exerted by the mouse. The animals were used to the test room and handled by only one researcher.

During the test, the experimenter gently manipulated the animals by the tail to allow adhesion of the animal with the front legs to the apparatus maintaining the body of the animal parallel to the surface. After holding for 2 s in this position, the experimenter continuously increased the force until the animals lost their grip. The peak of the force automatically recorded at the time the animals lost their adhesion was recorded and expressed in grams/force (g/f). The test was performed 3 times for each animal for a maximum period of 60 s. The mean values of three trials were calculated for each animal and used for further analysis.

### Statistical Analysis

We used Microsoft Excel for analyses and all data were plotted using the program GraphPad Prism 6. For data with normal distribution, values were represented as the standard error of the mean. Statistical significance was evaluated using the unpaired Student's *t* test. As described earlier, when data were not normally distributed, values were represented as the median, and the Mann–Whitney test was used to evaluate statistical significance. Values of  $p < .05$  were considered statistically significant. Exact *p* values were provided in the figure captions. During analysis, the investigators were blinded for both animal genotype and experimental group. A specific number was assigned to each of the genotyped animals, and the identifier was announced to the researchers only all the analyses were completed.

In this work, we used a minimum of three animals per genotype for each data set to obtain statistical difference with 95% of confidence ( $\alpha = 0.05$ ) and 0.8 power.

The exact  $n$  for each experimental procedure is described in the figures' captions.

## Results

### *Lumbar Spinal Cord Motoneurons Are Reduced in Size and Number and Are Caspase Positive in BACHD Mice*

Reduced lower limb muscle strength has been described in HD patients and this contributes significantly to mobility and balance problems in HD (Busse et al., 2008; T. Cruickshank et al., 2014). Herein, we investigated whether the lumbar spinal cord motoneurons that innervate lower limb muscles are affected in 12-month-old BACHD mouse model for HD.

We began by investigating the number, size, and morphology of the motoneurons from the ventral spinal cord lumbar segments (L1–L5). Figure 1(a) and (b) shows representative images of ChAT-positive (a motoneuron marker) neurons located in the ventral portion of the lumbar segments of the spinal cord of WT and BACHD animals, respectively. Quantitative analysis of ChAT-positive neurons showed a significant decrease in the total number of ChAT-positive cells in the lumbar segments of BACHD animals when compared with WT animals (BACHD:  $142.0 \pm 8.0$  number; WT:  $178.0 \pm 17.6$  number, mean  $\pm$  standard deviation [ $SD$ ];  $T_4 = 3.3$ ;  $*p < .02$ ; Figure 1(e)). We also noticed a significant decrease in the diameter of these neurons, with ChAT-positive-BACHD neurons being smaller than WT (BACHD:  $23.7 \pm 2.0$   $\mu\text{m}$ ; WT:  $28.3 \pm 1.4$   $\mu\text{m}$  [mean  $\pm$   $SD$ ];  $T_4 = 3.1$ ;  $*p < .03$ ; Figure 1(f)). A similar trend in number and size was observed when the antibody against OPN (a specific marker for alpha motoneuron type) was used in the lumbar spinal cord segments. A statistically significant decrease in the number (BACHD:  $80.5 \pm 25.3$  number; WT:  $131.0 \pm 31.4$  number [mean  $\pm$   $SD$ ];  $T_6 = 2.5$ ;  $*p < .02$ ) and diameter (BACHD:  $30.2 \pm 2.3$   $\mu\text{m}$ ; WT:  $35.1 \pm 0.6$   $\mu\text{m}$ ;  $T_4 = 3.5$ ;  $*p < .02$ ) of OPN-positive neurons was observed in BACHD mice compared with WT (Figure 1(g) and (h)).

It is possible that BACHD ChAT/OPN-positive neurons were dying at 12 months old. Thus, we immunostained lumbar spinal cord sections (40  $\mu\text{m}$ ) of BACHD and WT animals for caspase-3 to investigate whether these motoneurons were undergoing apoptosis. Figure 1(c) shows representative images of WT lumbar segments incubated with the antibody anticaspase-3. Very little caspase staining was observed in all WT lumbar sections. On the other hand, lumbar spinal cord sections of BACHD animals showed a clear presence of caspase-3 labeling with the majority was in ventral horn neurons, mostly in motoneurons (white arrows; Figure 1(d)).

These observations were confirmed by quantitative analyses of several lumbar spinal cord sections for both genotypes (BACHD:  $65.6 \pm 8.3$  number; WT:  $27.0 \pm 4.3$  number [mean  $\pm$   $SD$ ];  $T_4 = 7.1$ ;  $**p < .002$ ; Figure 1(m)). Overall, these results indicate that the activation of the apoptotic cascade can be part of the degenerative changes seen in motoneurons of BACHD animals.

We next asked if motoneurons from BACHD lumbar spinal cord presented any abnormal feature at the ultra-structure level. Qualitative analysis of electron micrographs showed that typical motoneurons in WT animals were large in size (Figure 1(i)), whereas motoneurons from BACHD animals looked significantly smaller (Figure 1(j), compare with Figure 1(i)). At the subcellular level, we observed abnormalities in the mitochondria from BACHD lumbar spinal cord motoneurons, such as cristae disruption and presence of vacuoles (Figure 1(l), yellow arrows), whereas in WT animals, this organelle was well preserved (Figure 1(k)). We also identified the presence of lipofuscin granules in motoneurons from BACHD (Figure 1(j)) and WT (Figure 1(i)) animals (red arrows). However, the number of these granules was not significantly different between the genotypes (BACHD:  $0.17 \pm 0.05$   $\mu\text{m}^2$ ; WT:  $0.17 \pm 0.03$   $\mu\text{m}^2$  [mean  $\pm$   $SD$ ];  $T_4 = 0.08$ ;  $p = .4$ ; Figure 1(n)).

### *Abnormalities in Sciatic Nerve and NMJs From BACHD Mice*

We next performed histological analysis of the sciatic nerve, which projects to the lower hind limb TA muscle (Figure 2(a) and (b)). We found statistically significant differences in the following morphological parameters between BACHD and WT mice: (i) axon diameter (BACHD:  $10.9 \pm 3.5$   $\mu\text{m}$ ; WT:  $11.4 \pm 4.02$   $\mu\text{m}$  [median];  $**p < .001$ ) (e); (ii) axoplasm diameter (BACHD:  $6.8 \pm 2.6$   $\mu\text{m}$ ; WT:  $7.5 \pm 2.8$   $\mu\text{m}$  [median];  $***p < .0001$ ) (f), and (iii)  $G$  ratio (BACHD:  $0.65 \pm 0.06$ ; WT:  $0.61 \pm 0.07$  [median];  $****p < .0001$ ) (h). However, no significant differences were observed between WT and BACHD sciatic nerves in terms of nerve area (c), number of axons per area (d), and myelin thickness (g).

To determine whether the sciatic nerve abnormalities described earlier were accompanied by changes in the innervation of the TA muscle, the NMJs of both genotypes were pre- and postsynaptically stained with synaptotagmin and  $\alpha$ -btx, respectively. Figure 3(a) and (b) shows representative images of presynaptic nerve terminals stained with Alexa 488 antisynaptotagmin antibodies from WT and BACHD TA muscles, respectively. Figure 3(a') (WT) and (b') (BACHD) shows the postsynaptic AChRs stained with Alexa 555  $\alpha$ -btx. Figure 3(a'') (WT) and (b'') (BACHD) shows the merge of both green and red signals. Figure 3(c) and (d) shows the graphic representation of the particle analysis for NMJs

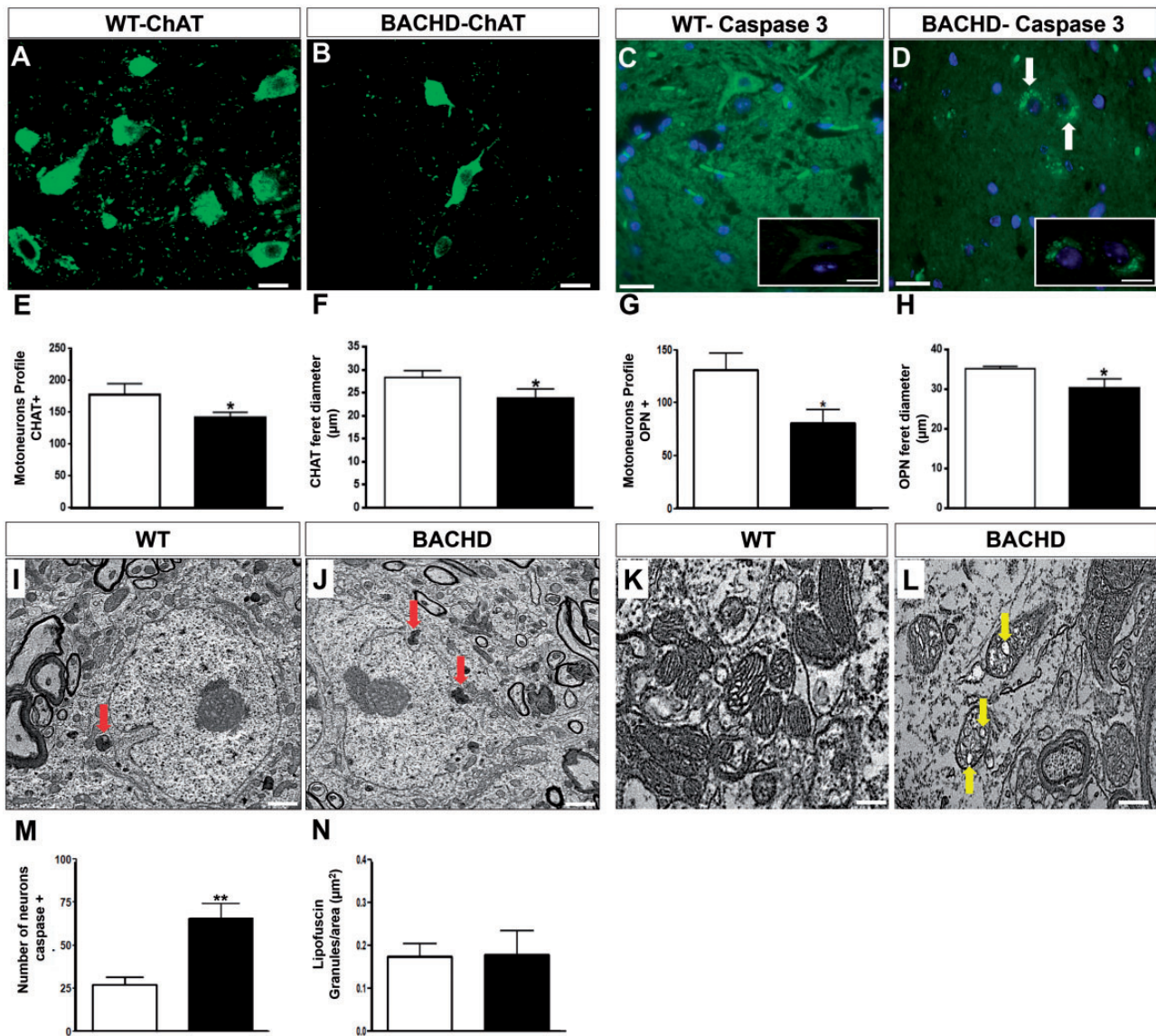


**Figure 1.** Atrophy in BACHD lumbar motoneurons. Representative images of motoneurons from lumbar spinal cord sections stained with ChAT from 12-month-old WT (a) and BACHD (b) animals. Scale bar: 50  $\mu\text{m}$ . Fluorescence images of putative motoneurons stained with caspase-3 in WT (c) and BACHD (d—white arrows). Nuclei were stained with 4',6-diamidino-2-phenylindole. Insert: putative motoneurons positive for caspase-3 in BACHD. Scale bar: 50  $\mu\text{m}$ . (e) and (g) Quantification of ChAT- and OPN-positive motoneurons profiles in WT and BACHD lumbar spinal cords ( $\sim 150$  neurons analyzed per genotype). Feret diameter for CHAT (f) and for OPN (h) (unpaired Student's *t* test;  $*p < .05$ ;  $n = 3$  animals per genotype). Ultrastructure images showing a motoneuron with more lipofuscin granules (red arrows) in BACHD (j) compared with WT (i). (k and l) Representative images normal and vacuolated mitochondria in WT and BACHD, respectively. Scale bar: 500 nm. (m) Graphical quantification of motoneurons stained positively for caspase-3 in WT and BACHD ( $\sim 150$  neurons analyzed per genotype; unpaired Student's *t* test;  $**p < .002$ ;  $n = 3$  animals per genotype). N: Quantification of the number of lipofuscin granules/area in WT and BACHD motoneurons (total from 30 motoneurons per genotype; unpaired Student's *t* test;  $p = .4$ ;  $n = 3$  animals per genotype). All results described here are from  $n = 3$  individual animals per genotype and were expressed as mean  $\pm$  SD. ChAT = choline acetyltransferase; WT = wild type.

fragmentation. Figure 3(c') and (d') shows the skeletonization process of the NMJs.

We found abnormal features in BACHD TA such as (i) loss of colocalization between pre- and postsynaptic elements (BACHD:  $87.5 \pm 0.8\%$ ; WT:  $93.1 \pm 1.2\%$  [mean  $\pm$  SD];  $T_4 = 3.6$ ;  $*p = .02$ ; Figure 3(e)); (ii) NMJs

partial denervation were identified considering their colocalization with nAChR clusters (BACHD:  $27.6 \pm 2.0\%$ ; WT:  $5.6 \pm 1.2\%$  [mean  $\pm$  SD];  $T_4 = 9.3$ ;  $***p = .0007$ ; Figure 3(f)); (iii) decreased presynaptic terminal area (BACHD:  $1,231 \pm 886 \mu\text{m}^2$ ; WT:  $1,761 \pm 964 \mu\text{m}^2$  [median];  $***p = .0002$ ), but not in postsynaptic area

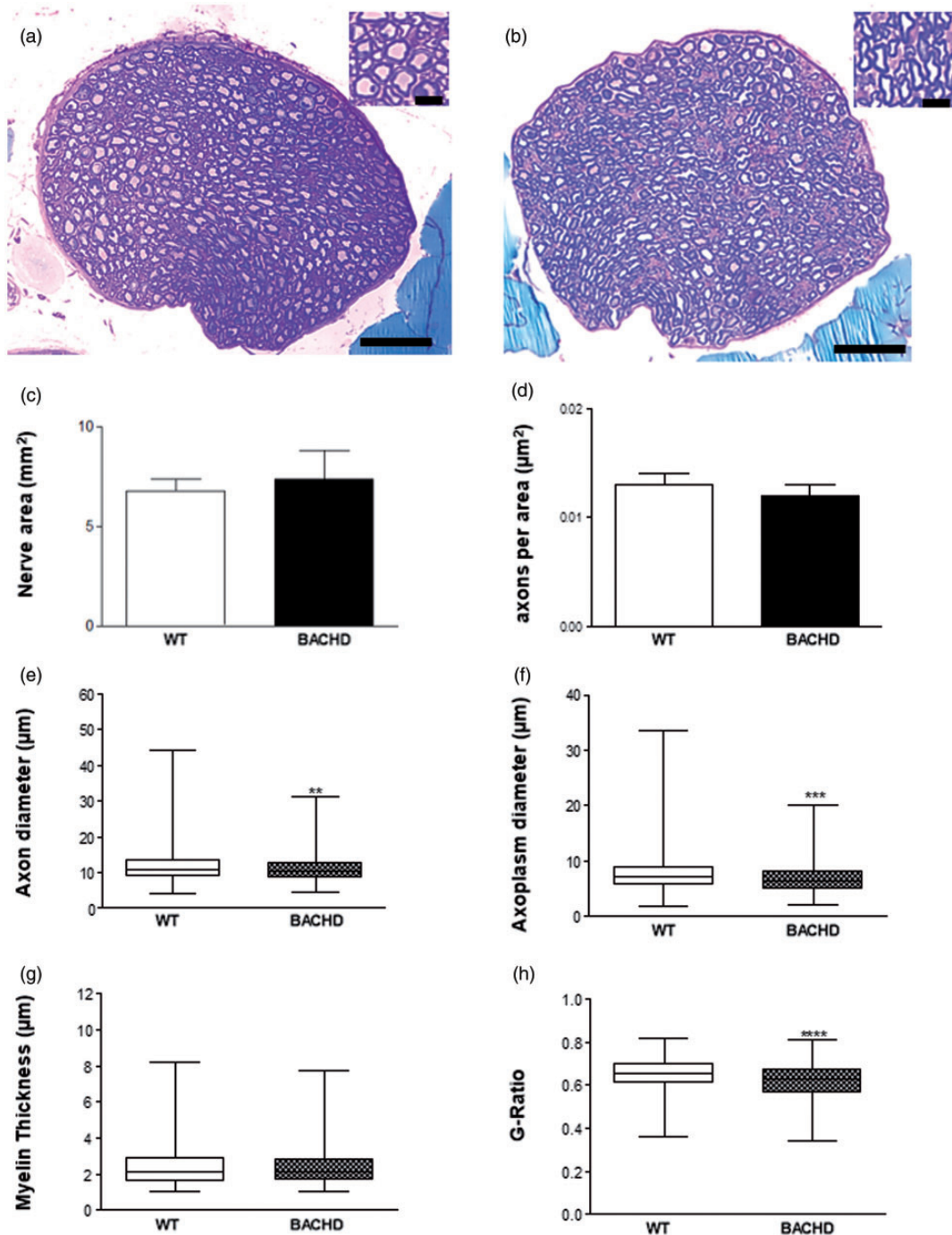


**Figure 2.** BACHD mice present alterations in sciatic nerve morphology. (a and b) Representative images of transversal sections of the sciatic nerve from 12-month-old WT and BACHD mice, respectively. Note the difference between the size of the axons in inserts in (a; WT) and (b; BACHD). Scale bar: 10  $\mu\text{m}$ . Quantification of nerve area (c), number of axons per nerve area (d), axon's diameter (e;  $**p < .001$ ; Mann–Whitney test), axoplasm diameter ( $***p < .0001$ ; Mann–Whitney test; f), myelin thickness (g), G ratio ( $G = d/D$ , where  $G$  is the G ratio,  $d$  is the inner diameter, and  $D$  is the outer diameter;  $****p < .0001$ ; Mann–Whitney test; h).  $n = 3$  animals per group. We analyzed 2.874 axons in WT and 2.573 in BACHD. Unpaired Student's  $t$  test,  $p > .05$  (c and d). WT = wild type.

(Figure 3(g) and (h)); and (iv) pronounced fragmentation of AChRs (BACHD:  $85.6 \pm 7.6 \mu\text{m}^2$ ; WT:  $47.6 \pm 3.5 \mu\text{m}^2$  [mean  $\pm$  SD];  $T_4 = 7.8$ ;  $**p = .001$ ; Figure 3(i)). We examined by western blot the expression of synaptotagmin (a

presynaptic marker) in WT and BACHD to confirm that the partial denervation seen was not due to decrease in synaptotagmin expression and BACHD animals at 12 months of age. We observed that the expression of

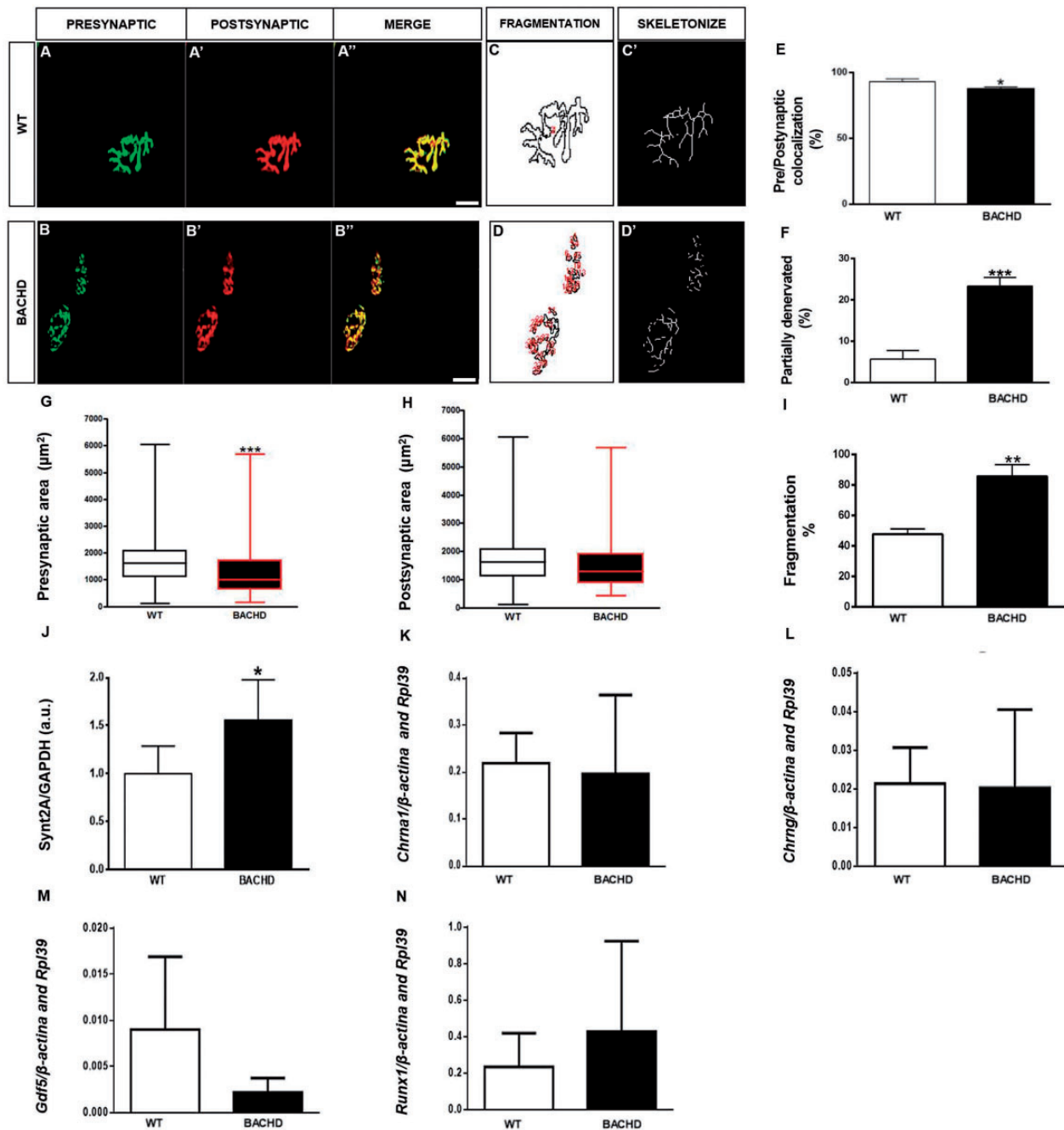


**Figure 3.** NMJs from TA muscles are partially denervated and fragmented in BACHD mice. (a and b) Representative images of TA NMJs obtained from 12-month-old WT and BACHD mice. (a and b) Presynaptic terminals labeled with an Alexa-488 antisynaptotagmin antibody (green). (a' and b') Postsynaptic AChRs labeled with Alexa-555  $\alpha$ -btx (red). (a'' and b''): merged images. Scale bar: 50  $\mu$ m. (c and d): representation of particle analysis for both genotypes (red numbers). (c' and d'): skeletonization rendering of fragmentation in endplates from WT and BACHD. Graphs showing the degree of colocalization (e) ( $*p = .02$ ; unpaired Student's *t* test); partial denervation (f) ( $***p = .0007$  unpaired Student's *t* test); presynaptic area (g) ( $***p = .0002$ ; Mann-Whitney test); postsynaptic area (h) ( $p > .05$ ; Mann-Whitney test); and fragmentation of the endplates (i) ( $***p = 0.001$ ; unpaired Student's *t* test). The results represent the mean  $\pm$  SD from 50 NMJs per genotype;  $n = 3$  individual animals per genotype. (j) Graphs showing higher expression of synaptotagmin in the TA muscle of BACHD mice. GAPDH was used as a control for protein loading. Densitogram analysis shows the normalized expression of synaptotagmin (Synt2a/GADPH) from WT and BACHD mice. The results described here are from  $n = 5$  animals per genotype and expressed as mean  $\pm$  SD. Unpaired Student's *t* test,  $*p = .04$ . Quantitative real-time polymerase chain reaction showing the expression of *chrn1* (k), *chrng* (l), *Gdf5* (m), and *runx1* (n) from TA muscle of WT and BACHD mice ( $n = 5$  per genotype group). Unpaired Student's *t* test,  $p > .05$ . Gene expression was normalized to the geometric mean of the following selected reference genes:  $\beta$ -actin and Rpl39. GAPDH = glyceraldehyde 3-phosphate dehydrogenase; WT = wild type.

synaptotagmin is even higher in the BACHD TA muscle than in the TA muscle of the WT animals (BACHD:  $1.5 \pm 0.4$ ; WT:  $1.0 \pm 0.2$  [mean  $\pm$  SD];  $T_8 = 2.4$ ;  $*p = .04$ ; Figure 3(j)). We also study the expression level of several genes known to change during denervation like *Chrna1* (Yu and Hall, 1991; Ibebunjo et al., 2013), *chrng*, *Gdf5* (Sartori et al., 2013) and *Runx1* (Zhu et al., 1994). Interestingly, we observed that there was no difference in any of the genes tested (Figure 3(k) to (n)).

All abnormalities described earlier were augmented in BACHD NMJs but were absent or present only in few cases in WT NMJs. All these analyses provided evidence of the degenerative process that is taking place at the NMJs of TA muscles from BACHD animals.

### **BACHD TA Muscle Fibers Are Atrophic, With Fiber-Type Switching and Show Signs of Degeneration at the Ultrastructure Level**

We investigated whether TA muscles, innervated by motoneurons from lumbar spinal cord segments, were affected in BACHD mice. To address this, cross-sections of TA muscles were stained with toluidine blue. Figure 4(a) and (b) shows representative images of TA muscle fibers from WT and BACHD animals, respectively. Quantitative analysis showed that the CSA of TA muscle fibers was smaller in BACHD mice compared with WT (Figure 4(k); BACHD:  $1,535 \pm 820.4 \mu\text{m}^2$ ; WT:  $1,965 \pm 7,794 \mu\text{m}^2$  [median];  $****p < .0001$ ). Ultrastructural analyses showed that WT-TA muscle fibers presented normal looking organelles such as mitochondria, well-preserved sarcomeres, triads, and myofibrils (yellow rectangle, Figure 4(e)). However, the BACHD-TA muscle fibers were different in structure, showing severely disorganized sarcomeres (Figure 4(f)—dotted area). Figure 4(g) shows an enlarged view of the dotted area indicated in Figure 4(f). Here, we observed atypical amounts of intermyofibrillar glycogen (red arrow), loss of alignment among the sarcomeres (blue arrows), and invasion of the sarcoplasmic reticulum onto the myofibrils region (yellow asterisk). In addition, large vacuoles within the mitochondrial matrix were observed in the mitochondria of BACHD muscle fibers, a feature typically present in mitochondria enrolled in degeneration (Figure 4(h) to (j)).

Next, we investigated whether the BACHD muscle atrophy could be associated to changes in myosin heavy chain (MyHC) isoforms expression. To evaluate this, we used immunostaining for different fiber types through specific monoclonal antibodies against various MyHC isoforms. The top panel represents staining for Type I (Figure 4(c)), Type IIA (Figure 4(c')), Type IIX (Figure 4(c'')), and Type IIB (Figure 4(c''')) isoforms of muscle fibers from WT animals. The bottom panel shows the same staining but in this case for muscle fibers from

BACHD animals (Figure 4(d') to (d''')). Quantitative analysis from individual animals showed a statistically significant decrease in the number of Type IIB fibers (BACHD:  $35.4 \pm 5.1\%$ ; WT:  $46.8 \pm 4.0\%$  [mean  $\pm$  SD];  $T_6 = 3.4$ ;  $*p < .01$ ) and an increase in the number of Type IIX muscle fibers (BACHD:  $48.3 \pm 8.3\%$ ; WT:  $32.5 \pm 5.9\%$  [mean  $\pm$  SD];  $T_4 = 3.0$ ;  $*p < .02$ ) in BACHD TA muscles (Figure 4(l)). Figure 4(m) shows that muscle fibers positive for Type IIX and Type IIB isoforms presented a decrease in fiber size (IIX: BACHD:  $381.5 \pm 171.9 \mu\text{m}^2$ ; WT:  $414.5 \pm 173.3 \mu\text{m}^2$  [mean  $\pm$  SD];  $T_{61} = 2.3$ ;  $*p < .03$ ; IIB: BACHD:  $634.3 \pm 238.6 \mu\text{m}^2$ ; WT:  $672.3 \pm 243.7 \mu\text{m}^2$  [mean  $\pm$  SD];  $T_{70} = 2.0$ ;  $*p < .03$ ).

### **Impaired Motor Behavior in BACHD Mice**

Based on the nerve–muscle alterations described earlier, we examined if BACHD mice indeed showed motor impairment. To assess the motor performance, mice from both genotypes were subjected to the following tests: paw print, wire hanging, grip strength, and open field. Regarding the paw print test data, we did not find significant differences between WT and BACHD for any of the evaluated standards: step length, step width, and right/left pass (Figure 5(a) to (d)). In the open-field test, BACHD mice showed a significant decrease in exploratory behavior. For example, the average distance traveled by BACHD mice was significantly shorter than the distance traveled by the WT mice (BACHD:  $133.1 \pm 59.8$  cm; WT:  $276.4 \pm 94.6$  cm [mean  $\pm$  SD];  $T_{26} = 4.92$ ;  $p < .001$ ; Figure 5(a)). In addition, the BACHD mice scored worse than WT regarding the mean velocity traveled (BACHD:  $0.10 \pm 0.30$  cm/s; WT:  $0.22 \pm 0.07$  cm/s [mean  $\pm$  SD];  $T_{26} = 5.52$ ;  $p < .001$ ; Figure 5(b)). The wire hanging task revealed that BACHD mice presented more difficulty in sustaining their weight, while most WT mice kept hold of the grid over the entire duration of the test (60 s; BACHD:  $0.4 \pm 0.09$  s; WT:  $1.4 \pm 0.09$  s [mean  $\pm$  SD];  $T_{27} = 7.2$ ;  $p < .0001$ ; Figure 5(c)). However, we did not observe significant differences in the grip strength test between the two genotypes BACHD and WT mice (i.e., test to compare maximum strength; Figure 5(d)).

## **Discussion**

Although HD is mostly described as a neurological disorder, there is growing evidence that a peripheral pathology participates in disease progression (Ribchester et al., 2004; van der Burg et al., 2009; Mielcarek, 2015). Indeed, HTT is normally expressed at high levels in a wide variety of mammalian tissues (Li et al., 1993) and pathological aggregates of high-molecular weight HTT have been found in many non-CNS tissues including skeletal muscle (Moffitt et al., 2009). Recently, we have showed

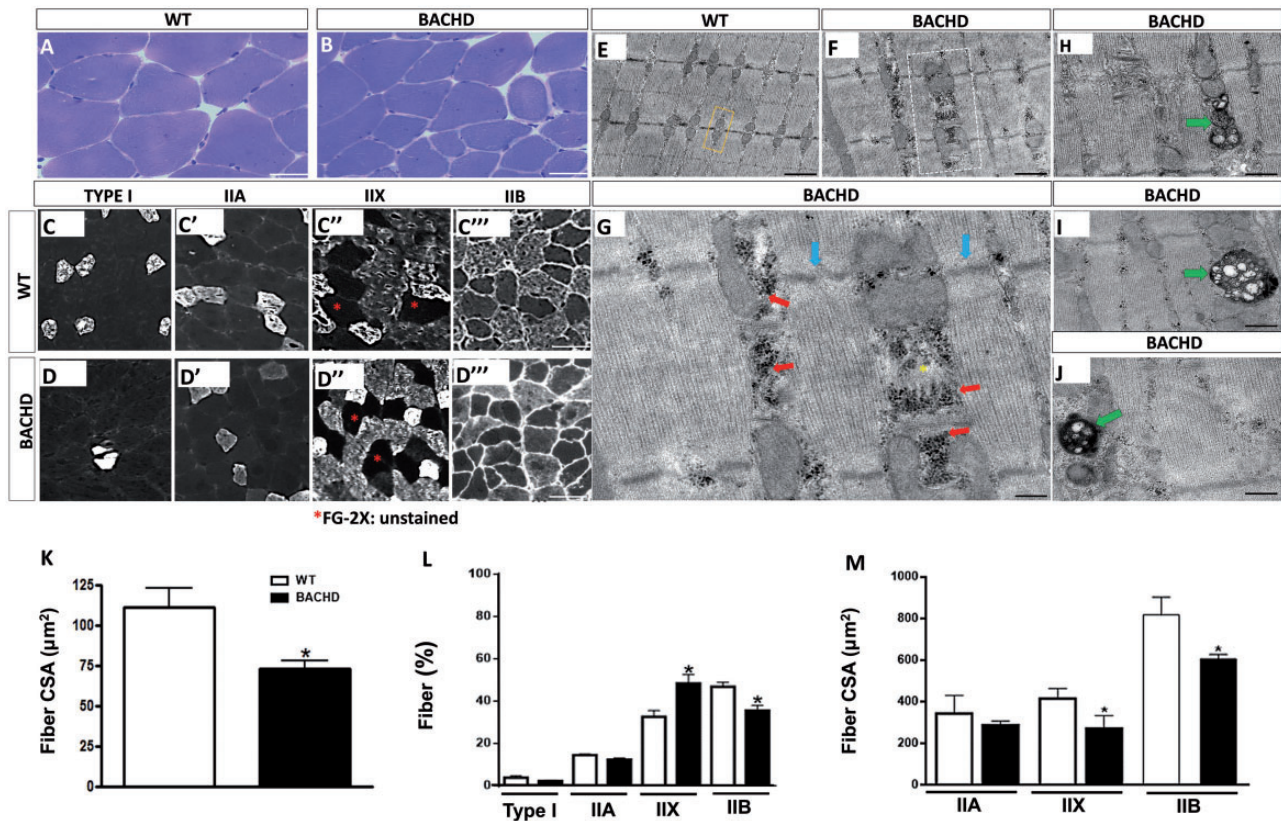


**Figure 4.** Muscle atrophy, muscle fiber switching and ultrastructural abnormalities in BACHD. (a and b) Representative images of TA skeletal muscle fibers from 12-month-old WT and BACHD mice. Scale bar: 50  $\mu\text{m}$ . (c to c'') and (d to d'') Representative images of TA fiber typing from 12-month-old WT and BACHD mice. Scale bar: 50  $\mu\text{m}$ . (e to j) Representative electron micrographs of TA fibers from WT and BACHD animals. Observe a normal triad in WT (e, yellow box). (g) High-magnification view of the area in (f) showing marked glycogen accumulation in the intermyofibrillar spaces (red arrows), sarcoplasmic reticulum enlargement (yellow asterisk) and Z-line discontinuity (blue arrows) in BACHD animals. (h to j) Observe profound mitochondrial changes (green arrows). Scale bar: 500 nm. We analyzed 90 images per genotype from six individual animals (three per genotype). (k) Quantitative analysis shows the CSA mean values for WT and BACHD TA muscle fibers. These results represent the mean  $\pm$  SD of more than 4,000 muscle fibers per genotype ( $*p < .04$ ; unpaired Student's *t* test;  $n = 3$  animals per genotype). (l) Quantitative analysis of the fiber typing showing decreased number of IIB isoform and increase of IIX in BACHD TA muscle fibers compared with WT ( $*p = .01$  and  $*p = .02$ ; unpaired Student's *t* test;  $n = 3$  animals per genotype). (m) Quantitative analysis of the CSA from fiber typing ( $*p = .03$ ; unpaired Student's *t* test;  $n = 3$  animals per genotype). The results represent the mean  $\pm$  SD (unpaired Student's *t* test,  $*p < .05$ ;  $n = 3$  animals per genotype). CSA = cross-sectional area; WT = wild type.

that MUs of a neck muscle (STM) from BACHD mice presented morphological alterations in all its components, that is, motoneurons, axons, NMJs, and muscle fibers (Valadão et al., 2017). Nevertheless, the connection between HD and the progressive disruption of communication between motoneurons and skeletal muscles remains poorly explored. Thus, in this study, we investigated whether similar changes were also present in MUs of the hind limb muscles such as the TA, which is controlled by lumbar spinal cord segments and afflicted by many degenerative disorders, including HD.

Previous works from other groups reported changes in NMJs and muscles in R6/2 mouse model for HD that could be related to motoneurons degeneration (Ribchester et al., 2004; Mielcarek and Isalan, 2015;

Khedraki et al., 2017). However, these authors did not look at the spinal cords to address whether motoneurons were indeed affected in R6/2 mice. In our previous work using the BACHD mouse model for HD, we examined this hypothesis. We observed that CHAT-positive neurons from BACHD cervical spinal cord segments were significantly fewer ( $\sim 20\%$ ) and smaller in size than those in WT mice (Valadão et al., 2017). In the current work, we showed, in another segment of the spinal cord (lumbar, L1–L5), that ChAT-positive neurons from BACHD lumbar segments were also fewer (motoneurons number) and smaller (cell soma diameter) compared with WT mice. Comparatively, these results show similar pathological changes among cervical and lumbar spinal cord segments in BACHD mice of the same age,

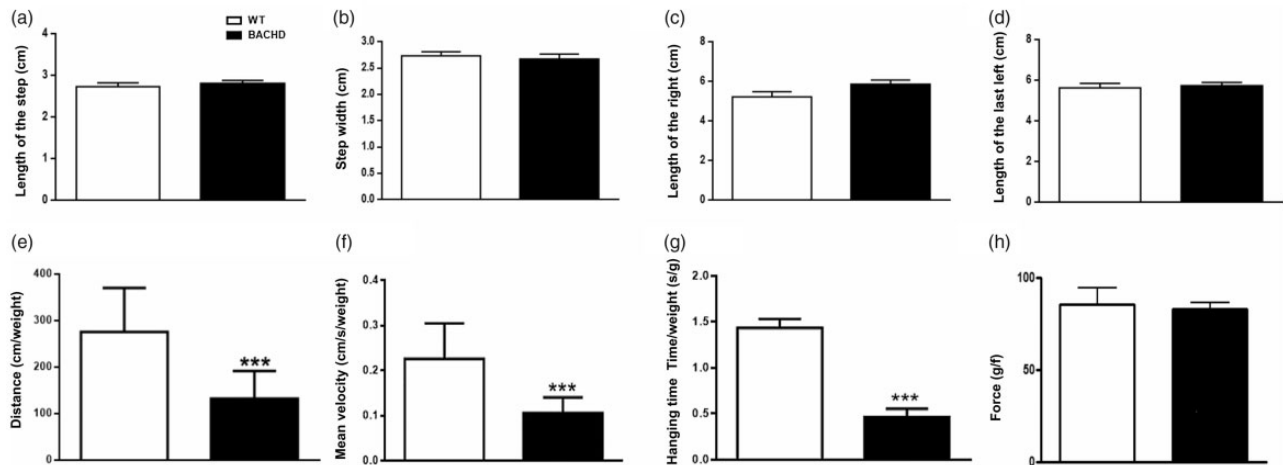


**Figure 5.** Motor behavior alterations in BACHD. (a to d) Graphical quantification of pattern of gait of WT and BACHD mice. (a) Length of the step ( $p = .54$ ; unpaired Student's  $t$  test). (b) Step width ( $p = .51$ ; unpaired Student's  $t$  test). (c) Length of the right ( $p = .07$ ; unpaired Student's  $t$  test). (d) Length of the left ( $p = .70$ ; unpaired Student's  $t$  test). (e) Graphical quantification of the total distance traveled by WT and BACHD mice, showing hypoactivity in transgenic animals (time/weight = time corrected for weight) (\*\*\* $p < .01$ ; unpaired Student's  $t$  test). (f) Graphical quantification of the average speed traveled by both genotypes with a decrease in BACHD animals (time/weight = time corrected for weight) (\*\*\* $p < .001$ ; unpaired Student's  $t$  test). (g) Graphical quantification of the total time the animals kept holding their own weight in the test apparatus (time/weight = time corrected for weight) (\*\*\* $p = .0001$ ; unpaired Student's  $t$  test). (h) Maximum force quantification in the test of grip strength exerted by WT animals and BACHD when a constant and opposite force is applied ( $p = .39$ ; unpaired Student's  $t$  test). The results express the mean  $\pm$  SD from 11 WT and 17 BACHD animals. GAPDH = glyceraldehyde 3-phosphate dehydrogenase; WT = wild type.

suggesting that both spinal cord segments (cervical and lumbar) undergo the same degree of impairment.

As in the cervical spinal cord segments (Valadão et al., 2017), here we observed that BACHD lumbar spinal cords present approximately 3 times more motoneurons positive for caspase-3 when compared with equivalent WT spinal segments. Although it is not completely clear whether the neuronal death seen in HD is due solely to apoptotic process, several lines of evidence indicate that the activation of specific pathways can lead to neuronal death (Hickey and Chesselet, 2003). In fact, Gervais et al. (2002), demonstrated that one of the neuronal death pathways in HD occurs through the interaction of mHTT with specific molecules that activate caspase-8, which in turns lead to mitochondrial alterations with consequent activation of caspase-3, culminating in cell death by apoptosis.

The qualitative analysis of electron micrographs of putative motoneurons (large ventral horn neurons) from BACHD animals presented herein revealed mitochondria with changes such as destruction of mitochondrial cristae and vacuoles. These subcellular changes were similar to those identified in BACHD cervical motoneurons (Valadão et al., 2017). In addition, we observed lipofuscin granules in both lumbar genotypes WT and BACHD. However, this observation was different from the cervical segments where we detected almost 3 times more lipofuscin granules in BACHD compared with WT

(Valadão et al., 2017). Studies using transmission electron microscopy to evaluate damages in the brain of HD patients have pointed out morphological alterations such as mitochondria with damaged cristae, occasionally containing crystalline fibrillar structures within the matrix and increase in lipofuscin granules (Tellez-Nagel et al., 1974; Goebel et al., 1978). Moreover, it has been shown that the relationship of mHTT with mitochondrial components leads to changes in its structure (Bossy-Wetzel et al., 2008; Song et al., 2011; Shirendeb et al., 2012).

Although we observed a decrease in the number of motoneurons, interestingly, the number of axons is not altered in BACHD animals. However, we have shown changes in both the axon and axoplasm diameter, which leads us to believe that these changes might be an earlier step in the process of total axonal degeneration.

Our results also showed changes in the NMJs of TA muscles at 12 months old in the BACHD animals. In this muscle, we identified a significant decrease in presynaptic element area, but not in the postsynaptic element, which may be explained by an initial denervation process, as we also observed locations where there was a lack of overlap between the presynaptic terminal and nAChR.

Furthermore, we identified significant fragmentation of NMJs of BACHD animals but little in control animals. Although recent data show that the age-

fragmentation process is not directly related to function (Willadt et al., 2016), we believe that our data may indicate that structural changes such as fragmentation are due to the genotype and not just related to age because the animals evaluated were of the same age. It is known that mHTT interacts with cytoskeletal synaptic vesicles proteins that are essential for the structure of NMJs and for exocytosis and endocytosis of synaptic vesicles at the nerve terminals (Li and Li, 2004; see review by Zuccato et al., 2010). Except for postsynaptic area size, which was not statistically different for the TA muscle, all these morphological changes were also observed in NMJs of STM muscle from 12-month-old BACHD animals. This comparison is useful because we are dealing with NMJs of two distinctive muscle groups that are affected differently in animals of the same age in the BACHD murine model for HD.

We do not observe changes in the number of axons in the sciatic nerve, despite the significant changes in the axons diameter. This result seems contrary to the loss of motoneurons (~20%) observed in the lumbar segments of the BACHD mice. There are several plausible explanations for this difference. It is possible that axonal degeneration is a much slower process than the caspase labeling observed at the spinal cord. This possibility finds support in the fact that axons stay for much longer than motoneurons, a phenomenon previously observed in amyotrophic lateral sclerosis disease, which is consistent with the lower number of partial denervation observed (10%). Another possibility is that the remaining motoneurons, the caspase negative, are able to produce new branches, which should travel within the nerve. These extra branches should account for a higher number of axons at the sciatic nerve level. As they are ramifications from the main axonal branch, most of the new branches should be smaller in size. This is consistent with the variability in axonal diameter observed in our sciatic nerve analysis.

Overall, our results do not show significant differences in terms of expression for any of the genes examined. It is possible that the level of partial denervation observed in BACHD mice, which accounts for about ~10% of the junctions of the TA muscle, is not enough to induce significant changes in the expression of the genes selected. It may also be possible that diverse signaling pathways are still in place controlling the expression of these genes. Whatever the case, these questions do not fall within the scope of our work. Our results also show that there is no decrease in synaptotagmin protein in NMJs of BACHD mice; on the contrary, this protein is overexpressed in these animals. These results reinforce that our denervation data were not due to possible alterations in the expression of the synaptotagmin protein.

Another interesting finding is the change observed in skeletal muscle fibers of the TA muscle from BACHD

mice. First, we observed a decrease in CSA in muscle fibers of BACHD animals suggesting muscle atrophy. A reduction in the total number of fibers could also have contributed to muscle fiber atrophy in the BACHD mouse. Indeed, it is well described that muscle atrophy is a common factor in HD (Farrer and Meaney, 1985; Ribchester et al., 2004; Farrer, 2008). Another point to be considered is the deleterious effects of mHTT in muscle fibers of R6/2 mice (Sathasivam et al., 1999; Moffitt et al., 2009). The BACHD-STM muscle also showed atrophy of muscle fibers (Valadão et al., 2017). However, the atrophy seen in the BACHD-TA muscle was smaller compared with BACHD-STM muscle. However, the STM muscle has higher variability in fiber size mainly because it has mixed features of contractility, consisting of fast and slow fibers. In contrast, the TA muscle is a fast-twitch muscle, usually presenting about 87% of fast fiber Type IIB muscle fibers (Bloemberg and Quadriatero, 2012).

Previous studies revealed that muscle atrophy could be accompanied by changes in expression of MyHC (Brown and Hasser, 1996; Carvalho et al., 2003; Rice et al., 2005; Valadão et al., 2017). Here, we show that the number of Type IIB muscle fibers was reduced in BACHD mice, indicating that the general atrophy seen in this muscle relates to a change in MyHC isoform because in TA muscle, Type IIB fibers are predominant (Bloemberg and Quadriatero, 2012). These data are in agreement with the work of Miranda et al. (2017) in which they showed the same pattern of transition of the type of fiber in the TA muscle of animals R6/2; however, these authors did not investigate the protein expression of MyHC, showing these changes only at the mRNA level through the quantitative PCR technique. Besides that, we had already identified changes in the expression pattern of MyHC in the STM muscle with changes of Type IIX muscle fibers was reduced in BACHD mice (Valadão et al., 2017). Together, these results indicate that the atrophy seen in both muscles was accompanied by alterations in the expression of MyHC, differing only in the affected fast fiber type. The MyHC shift from Type IIB to Type IIX seen in BACHD TA muscle might be explained by the observation that, in denervated muscles, there is a change in the expression pattern of the faster isoforms for the slower isoforms (d'Albis et al., 1995). We speculate that this fiber type may be related to the NMJs denervation observed in the TA muscles from BACHD mice. Data from the literature indicate that motoneurons and their NMJs differ drastically in size, with biggest ones innervating fast muscle fibers with largest NMJs (Burke et al., 1971; Mantilla et al., 2007). We hypothesize that the changes in the motoneurons described herein, such as decrease in presynaptic area and size of motoneurons in BACHD, cause a reduction in the number of IIB muscle fibers in TA muscles from BACHD mice.

However, we cannot rule out the possibility that mHTT directly or indirectly alters muscle fiber-type profile as this has been described in R6/2 HD mice model and also in humans (Strand et al., 2005; for a review, see Zielonka et al., 2014). Further research will be needed to clarify this matter.

Interestingly, we noted that the BACHD-TA muscles have greater accumulation of glycogen in the intermyofibrillar spaces and more mitochondrial damage than the observed in STM muscles (Valadão et al., 2017). Moreover, in the BACHD transgenic animals, the Z line did not follow a straight pattern as observed in the control animals. Indeed, studies of denervated TA muscles of transgenic rabbits also revealed Z-line misalignment and mitochondrial changes (Ashley et al., 2007). In light of the information provided by these studies and because we found greater changes in the mitochondria of BACHD TA muscles, it is possible that these changes could be related to energy imbalance caused by mitochondrial damage. However, it is important to mention that although the transmission electron microscopy analysis revealing mitochondrial abnormalities is informative, caution should be taken in the interpretation of the present data because our analysis was only qualitative and not quantitative.

We evaluated the motor function of BACHD and WT mice to verify the possible relationship between the morphological changes observed in TA MUs and the alterations in motor behavior of BACHD animals. In the catwalk test, we did not detect statically significant differences between WT and BACHD mice in any of the gait patterns evaluated: step length, step width, and right/left pass. Interestingly, our results are in accordance with the data of Mantovani et al. (2016), who showed no significant differences in walking test between BACHD animals and controls at 12 months old, even using another measuring device (Noldus® Cat Walk apparatus [Wageningen, the Netherlands]). These observations may be related to the fact that the mice are quadruped animals, which gives them greater stability. Interestingly, L. Menalled et al. (2009) using the same method used by us, observed that 18-month-old BACHD mice presented statistical differences as a larger extension and broader base. These changes differ from the gait deficit found in humans, as the steps become shorter in patients with HD (Koller and Trimble, 1985). However, even without presenting significant changes in the gait, the 12-month-old BACHD mice showed a robust phenotype in several behavioral tests that replicate and extend the published results to date (Gray et al., 2008; L. Menalled et al., 2009; Mantovani et al., 2016).

The open-field test revealed significant hypoactivity of BACHD mice, with a significant reduction in locomotion, total distance traveled, and mean velocity. However, the number of rearing events was not

significantly different when compared with control mice. These findings are in accordance with the results reported by L. Menalled et al. (2009), which showed that at 7 months of age, BACHD mice presented locomotor hypoactivity. The same results (in 7-month-old BACHD) were previously observed by Gray et al. (2008). In the wire hanging test, we observed that BACHD mice performed significantly worse than the WT mice, similar to what Heng et al. (2007) and Brooks et al. (2012) noticed in 12-month-old *Hdh*<sup>(CAG)<sup>150</sup></sup> mice. In the wire hanging test, we observed that BACHD mice performed worse than the WT mice even after normalizing the weight of the animals to the time they were kept holding to the apparatus. It is known that BACHD FVB/N-Tg (HTT\*97Q) IXwy/J mice have increased body weight with age (Gray et al., 2008). According to Mantovani et al. (2016), female and male BACHD C57BL/6J mice gain significantly more weight over time, whereas females show a 35% increase in body weight and males have a 15% increase when compared with their WTs. For this reason, we normalized the weight of the animals to the time they were kept holding to the apparatus. Regarding the open-field test, we did not make this correction, because although body weight may influence this test, literature data show that after food restriction, WT and BACHD animals at 95 weeks of age present significant differences between the genotypes in the distance traveled, even after food restriction (Kudwa et al., 2013). In fact, the animals became more active after food restriction; however, these results may have been influenced by the fact that dietary restriction may alter the level of anxiety in mice by making them more active in the open-field test, which generates a false impression that weight loss can improve the motor performance of these animals (Wable et al., 2015).

In sum, the results obtained showed that the BACHD mice has major motor alterations, which directly influence their behavior. The grip strength test did not show significant changes in the maximum strength between BACHD and WT mice. L. Menalled et al. (2009) observed that mice containing only a fragment of mutant HTT (R6/2) showed deficits in the same motor test. However, animals expressing the full-length mHTT, including BACHD, showed no significant differences in grip strength test. Accordingly, Mantovani et al. (2016) showed that BACHD animals generated in a C57BL/6J background (12 months old) did not present deficits in grip strength test, which corroborate our results. It is also possible that the deficiencies in movement and balance observed are due to aberrant connectivity or function in motor systems of the brain, rather than brain stem or spinal motor neurons. Besides that, this test is also open to interpretation as motivational rather than NMJ/muscle physiological. Therefore, the case for NMJ involvement in motoneuron/muscle atrophy

would be better made from isometric force measurements and intracellular measurements of synaptic function.

Although the findings described herein are suggestive of axonal or NMJ morphological differences in the BACHD mouse model, future research involving corroborative nerve conduction measurements, muscle/MU tension data, or electrophysiological analysis of NMJ function are necessary to establish whether the abnormalities described at NMJs are biologically significant or whether they are primary consequences of CAG repeat expression or a secondary change in response to, for example, muscle atrophy.

It is important to note that all these results were obtained from 12-month-old WT and BACHD males. However, we judge that a study using females would be valuable, as HD is a disease that affects both sexes and it has already been shown that this disease has slightly faster progression in females than in males (Zielonka et al., 2013). In addition, in a recent study, Zielonka et al. (2018), showed that women with HD have a declining motor function affecting, more severely, on functionality and independence than in men. On the other hand, an elegant study was conducted using the HdhQ350/+ HD mice line, demonstrating that expanded polyglutamine repeats influence the pathogenesis of HD in a sex-dependent manner in these mice (Cao et al., 2018). The results show that only HdhQ350/+ males have impaired motor coordination and gait, while females show no impairment in motor coordination (Cao et al., 2018).

Therefore, in the face of these evidences in humans and the animal model for HD, we reiterate that it is in our interest, in future research, to analyze the entire MU in females WT and BACHD at 12 months of age, because in addition to the issues previously mentioned in relation to gender, females present the issue of the estrous cycle, a hormonal wildcard that might or might not bring other perspectives to our study. However, for reasons of creation, maintenance, conduction of experiments, equipment expenses, reagents and, finally, all the costs that a research of this level demands, we opted to carry out, first, a complete work in males.

In summary, here we show that that motoneurons from BACHD lumbar spinal cord are atrophic, reduced in size, and undergo apoptosis. The MUs associated with the TA muscle from BACHD mice present signs of degeneration such as sciatic nerve reduced axon and axoplasm diameters, NMJs' fragmentation and partial denervation, skeletal muscle fibers atrophy, and fiber-type switching (Type 2B–Type 2X). Moreover, this study provides evidence that different MUs have similar degrees of impairment in this animal model for HD. That is, regardless of innervation or muscle composition, it appears that mHTT may be performing the same degree of degeneration of these MUs investigated by us

in the two studies. In addition, the changes seen in different spinal cord segments indicate that, our results are in accordance with neuronal death in the brain. Therefore, the discovery that motoneurons at the lumbar spinal cord can be affected in HD, make room for further studies to elucidate the molecular mechanisms underlying the motoneuron cell death. Overall, our findings are important, and add further support to the hypothesis that cellular alterations occurring in peripheral tissues, in this case skeletal muscles, occur independently of the progression of brain dysfunction (van der Burg et al., 2009). Thus, this work expands the perspectives about the role of the MU in motor alterations seen in HD and the possibility that clinical interventions targeting the MU could help treating signs of disease in patients with HD.

## Summary

This study evaluates the morphology of the motor unit of the tibialis anterior muscle. The main finding is that Huntington's disease can affect the motor unit in all its components, from the motoneuron to the skeletal muscle.

## Author Contributions

P. A. C. V. was responsible for experimentation, data interpretation, and writing of the article. B. C. A., M. P. S. M.-G., J. N. A., G. F., I. C. G. J., J. M. N., R. S. P., E. C. J., S. G. and J. V. J.-S. were responsible for experimentation and data interpretation. T. C. G. M and L. P. were responsible for data analysis. J. C. N, F. M. R., and J. C. T. were scientific consultant in all the stages. C. G. was responsible for the conceptualization of the study data interpretation and writing the article.

## Acknowledgments

The authors would like to acknowledge the Center of Acquisition and Processing of Images at Instituto de Ciências Biológicas-Universidade Federal de Minas Gerais and Microscopy Center at Universidade Federal de Minas Gerais for providing the equipment and technical support for experiments involving electron microscopy. The authors would like to thank Dr. Dawit Gonçalves for advice on denervation genes.

## Declaration of Conflicting Interests

The author(s) declared no potential conflicts of interest with respect to the research, authorship, and/or publication of this article.

## Funding

The author(s) disclosed receipt of the following financial support for the research, authorship, and/or publication of this article: This work was supported by grants from Universidade Federal de Minas Gerais, Fundação de Amparo à Pesquisa do Estado de Minas Gerais, Conselho Nacional de Pesquisas

(CNPq) and Coordenação de Aperfeiçoamento de Pessoal de Nível Superior (to C. G.) and FONDECYT (1160888 and 1161014; to J. C. T.). C. G. is Bolsista de Produtividade em Pesquisa (CNPq).

### ORCID iDs

Fabiola Mara Ribeiro  <https://orcid.org/0000-0001-7042-9433>

Cristina Guatimosim  <https://orcid.org/0000-0001-5392-1266>

### References

- Ashley, Z., Salmons, S., Boncompagni, S., Protasi, F., Russold, M., Lanmuller, H., Mayr, W., Sutherland, H., & Jarvis, J. C. (2007). Effects of chronic electrical stimulation on long-term denervated muscles of the rabbit hind limb. *J Muscle Res Cell Motil*, *28*, 203–217. doi:10.1007/s10974-007-9119-4
- Bilney, B., Morris, M. E., Churchyard, A., Chiu, E., & Georgiou-Karistianis, N. (2005). Evidence for a disorder of locomotor timing in Huntington's disease. *Mov Disord*, *20*, 51–57. doi:10.1002/mds.20294
- Bloemberg, D., & Quadriatero, J. (2012). Rapid determination of myosin heavy chain expression in rat, mouse, and human skeletal muscle using multicolor immunofluorescence analysis. *PLoS One*, *7*, e35273. doi:10.1371/journal.pone.0035273
- Bossy-Wetzell, E., Petrilli, A., & Knott, A. B. (2008). Mutant huntingtin and mitochondrial dysfunction. *Trends Neurosci*, *31*, 609–616. doi:10.1016/j.tins.2008.09.004
- Brooks, S., Higgs, G., Jones, L., & Dunnett, S. B. (2012). Longitudinal analysis of the behavioural phenotype in Hdh(CAG)150 Huntington's disease knock-in mice. *Brain Res Bull*, *88*, 182–188. doi:10.1016/j.brainresbull.2010.05.004
- Brown, M., & Hasser, E. M. (1996). Complexity of age-related change in skeletal muscle. *J Gerontol A Biol Sci Med Sci*, *51*, B117–B123. doi:10.1093/gerona/51a.2.b117
- Burke, R. E., Levine, D. N., & Zajac, F. E. (1971). Mammalian motor units: Physiological-histochemical correlation in three types in cat gastrocnemius. *Science*, *174*, 709–12.
- Busse, M. E., Khalil, H., Quinn, L., & Rosser, A. E. (2008). Physical therapy intervention for people with Huntington disease. *Phys Ther*, *88*, 820–831. doi:10.2522/ptj.20070346
- Cao, J. K., Detloff, P. J., Gardner, R. G., & Stella, N. (2018). Sex-dependent behavioral impairments in the HdhQ350/+ mouse line. *Behav Brain Res*, *337*, 34–45. doi:10.1016/j.bbr.2017.09.026
- Carroll, J. B., Bates, G. P., Steffan, J., Saft, C., & Tabrizi, S. J. (2015). Treating the whole body in Huntington's disease. *Lancet Neurol*, *14*, 1135–1142. doi:10.1016/S1474-4422(15)00177-5
- Carvalho, R. F., Cicogna, A. C., Campos, G. E. R., De Assis, J. M. F., Padovani, C. R., Okoshi, M. P., & Pai-Silva, M. D. (2003). Myosin heavy chain expression and atrophy in rat skeletal muscle during transition from cardiac hypertrophy to heart failure. *Int J Exp Pathol*, *84*, 201–206. doi:10.1046/j.1365-2613.2003.00351.x
- Chau, W. K., So, K.-F., Tay, D., & Dockery, P. (2000). A morphometric study of optic axons regenerated in a sciatic nerve graft of adult rats. *Restor Neurol Neurosci*, *16*, 105–116.
- Cruickshank, T., Reyes, A., Peñailillo, L., Thompson, J., & Ziman, M. (2014). Factors that contribute to balance and mobility impairments in individuals with Huntington's disease. *Basal Ganglia*, *4*, 67–70. doi:10.1016/j.baga.2014.04.002
- Cruickshank, T. M., Thompson, J. A., Domínguez D, J. F., Reyes, A. P., Bynevelt, M., Georgiou-Karistianis, N., Barker, R. A., & Ziman, M. R. (2015). The effect of multidisciplinary rehabilitation on brain structure and cognition in Huntington's disease: An exploratory study. *Brain Behav*, *5*, e00312. doi:10.1002/brb3.312
- d'Albis, A., Couteaux, R., Goubel, F., Janmot, C., & Mira, J. C. (1995). Relationship between muscle myosin isoforms and contractile features in rabbit fast-twitch denervated muscle. *FEBS Lett*, *375*, 67–68.
- de Lagrán, M. M., Altafaj, X., Gallego, X., Martí, E., Estivill, X., Sahun, I., Fillat, C., & Dierssen, M. (2004). Motor phenotypic alterations in TgDyrk1a transgenic mice implicate DYRK1A in Down syndrome motor dysfunction. *Neurobiol Dis*, *15*, 132–142.
- Eisen, A., Kim, S., & Pant, B. (1992). Amyotrophic lateral sclerosis (ALS): A phylogenetic disease of the corticomotoneuron? *Muscle Nerve*, *15*, 219–224. doi:10.1002/mus.880150215
- Farrer, L. A. (2008). Diabetes mellitus in Huntington disease. *Clin Genet*, *27*, 62–67. doi:10.1111/j.1399-0004.1985.tb00185.x
- Farrer, L. A., & Meaney, F. J. (1985). An anthropometric assessment of Huntington's disease patients and families. *Am J Phys Anthropol*, *67*, 185–194. doi:10.1002/ajpa.1330670304
- Fischer, L. R., Culver, D. G., Tennant, P., Davis, A. A., Wang, M., Castellano-Sanchez, A., Khan, J., Polak, M. A., & Glass, J. D. (2004). Amyotrophic lateral sclerosis is a distal axonopathy: evidence in mice and man. *Experimental neurology*, *185*, 232–240.
- Fowler, S. C., Zarcone, T. J., Chen, R., Taylor, M. D., & Wright, D. E. (2002). Low grip strength, impaired tongue force and hyperactivity induced by overexpression of neurotrophin-3 in mouse skeletal muscle. *Int J Dev Neurosci*, *20*, 303–308.
- Gervais, F. G., Singaraja, R., Xanthoudakis, S., Gutekunst, C.-A., Leavitt, B. R., Metzler, M., Hackam, A. S., Tam, J., Vaillancourt, J. P., Houtzager, V., Rasper, D. M., Roy, S., Hayden, M. R., & Nicholson, D. W. (2002). Recruitment and activation of caspase-8 by the Huntingtin-interacting protein Hip-1 and a novel partner Hippi. *Nat Cell Biol*, *4*, 95–105. doi:10.1038/ncb735
- Goebel, H. H., Heipertz, R., Scholz, W., Iqbal, K., & Tellez-Nagel, I. (1978). Juvenile Huntington chorea: Clinical, ultrastructural, and biochemical studies. *Neurology*, *28*, 23–31.
- Gray, M., Shirasaki, D. I., Cepeda, C., Andre, V. M., Wilburn, B., Lu, X.-H., Tao, J., Yamazaki, I., Li, S.-H., Sun, Y. E., Li, X.-J., Levine, M. S., & Yang, X. W. (2008). Full-length human mutant huntingtin with a stable polyglutamine repeat can elicit progressive and selective neuropathogenesis in BACHD mice. *J Neurosci*, *28*, 6182–6195. doi:10.1523/JNEUROSCI.0857-08.2008

- Heng, M. Y., Detloff, P. J., & Albin, R. L. (2008). Rodent genetic models of Huntington disease. *Neurobiol Dis*, *32*(1), 1–9. doi:10.1016/j.nbd.2008.06.005
- Heng, M. Y., Tallaksen-Greene, S. J., Detloff, P. J., & Albin, R. L. (2007). Longitudinal evaluation of the Hdh(CAG)150 knock-in murine model of Huntington's disease. *J Neurosci*, *27*, 8989–8998. doi:10.1523/JNEUROSCI.1830-07.2007
- Hickey, M. A., & Chesselet, M.-F. (2003). Apoptosis in Huntington's disease. *Prog Neuropsychopharmacol Biol Psychiatry*, *27*, 255–265. doi:10.1016/S0278-5846(03)00021-6
- Ibeunjo, C., Chick, J. M., Kendall, T., Eash, J. K., Li, C., Zhang, Y., Vickers, C., Wu, Z., Clarke, B. A., Shi, J., Cruz, J., Fournier, B., Brachat, S., Gutzwiller, S., Ma Q., Markovits, J., Broome, M., Steinkrauss, M., Skuba, E., Galarneau, J. R., Gygi, S. P., & Glass, D. J. (2013). Genomic and proteomic profiling reveals reduced mitochondrial function and disruption of the neuromuscular junction driving rat sarcopenia. *Mol Cell Biol*, *33*, 194–212. doi:10.1128/MCB.01036-12
- Joviano-Santos, J. V., Santos-Miranda, A., Botelho, A. F. M., de Jesus, I. C. G., Andrade, J. N., de Oliveira Barreto, T., Magalhães-Gomes, M. P. S., Valadão, P. A. C., Cruz, J. dos S., Melo, M. M., Guatimosim, S., & Guatimosim, C. (2019). Increased oxidative stress and CaMKII activity contribute to electro-mechanical defects in cardiomyocytes from a murine model of Huntington's disease. *FEBS J*, *286*, 110–123. doi:10.1111/febs.14706
- Kazantsev, A., Preisinger, E., Dranovsky, A., Goldgaber, D., & Housman, D. (1999). Insoluble detergent-resistant aggregates form between pathological and nonpathological lengths of polyglutamine in mammalian cells. *Proc Natl Acad Sci*, *96*, 11404–11409.
- Khedraki, A., Reed, E., Romer, S. H., Wang, Q., Romine, W., Rich, M. M., Talmadge, R. J., & Voss, A. A. (2017). Depressed synaptic transmission and reduced vesicle release sites in Huntington's disease neuromuscular junctions. *J Neurosci*, *37*, 8077–8091.
- Koller, W. C., & Trimble, J. (1985). The gait abnormality of Huntington's disease. *Neurology*, *35*, 1450–1454. doi:10.1212/wnl.35.10.1450
- Kudwa, A. E., Menalled, L. B., Oakeshott, S., Murphy, C., Mushlin, R., Fitzpatrick, J., Miller, S. F., McConnell, K., Port, R., Torello, J., Howland, D., Ramboz, S., & Brunner, D. (2013). Increased body weight of the BAC HD transgenic mouse model of huntington's disease accounts for some but not all of the observed HD-like motor deficits. *PLoS Curr*, *5*, 1–14. doi:10.1371/currents.hd.0ab4f3645aff523c56ecc8ccbe41a198
- Li, S.-H., Schilling, G., Young, W. S., Li, X. J., Margolis, R. L., Stine, O. C., Wagster, M. V., Abbott, M. H., Franz, M. L., & Ranen, N. G. (1993). Huntington's disease gene (IT15) is widely expressed in human and rat tissues. *Neuron*, *11*, 985–993.
- Li, S.-H., & Li, X.-J. (2004). Huntingtin–protein interactions and the pathogenesis of Huntington's disease. *Trends Genet*, *20*, 146–154. doi:10.1016/j.tig.2004.01.008
- MacDonald, M. E., Ambrose, C. M., Duyao, M. P., Myers, R. H., Lin, C., Srinidhi, L., Barnes, G., Taylor, S. A., James, M., Groot, N., MacFarlane, H., Jenkins, B., Anderson, M. A., Wexler, N. S., Gusella, J. F., Bates, G. P., Baxendale, S., Hummerich, H., Kirby, S., North, M., Youngman, S., Mott, R., Zehetner, G., Sedlacek, Z., Poustka, A., Frischauf, A.-M., Lehrach, H., Buckler, A. J., Church, D., Doucette-Stamm, L., O'Donovan, M. C., Riba-Ramirez, L., Shah, M., Stanton, V. P., Strobel, S. A., Draths, K. M., Wales, J. L., Dervan, P., Housman, D. E., Altherr, M., Shiang, R., Thompson, L., Fielder, T., Wasmuth, J. J., Tagle, D., Valdes, J., Elmer, L., Allard, M., Castilla, L., Swaroop, M., Blanchard, K., Collins, F. S., Snell, R., Holloway, T., Gillespie, K., Datson, N., Shaw, D., & Harper, P. S. (1993). A novel gene containing a trinucleotide repeat that is expanded and unstable on Huntington's disease chromosomes. *Cell*, *72*, 971–983.
- Mantilla, C. B., Rowley, K. L., Zhan, W.-Z., Fahim, M. A., & Sieck, G. C. (2007). Synaptic vesicle pools at diaphragm neuromuscular junctions vary with motoneuron soma, not axon terminal, inactivity. *Neuroscience*, *146*, 178–189. doi:10.1016/j.neuroscience.2007.01.048
- Mantovani, S., Gordon, R., Li, R., Christie, D. C., Kumar, V., & Woodruff, T. M. (2016). Motor deficits associated with Huntington's disease occur in the absence of striatal degeneration in BACHD transgenic mice. *Hum Mol Genet*, *25*, 1780–1791. doi:10.1093/hmg/ddw050
- Menalled, L., El-Khodori, B. F., Patry, M., Suárez-Fariñas, M., Orenstein, S. J., Zahasky, B., Leahy, C., Wheeler, V., Yang, X. W., MacDonald, M., Morton, A. J., Bates, G., Leeds, J., Park, L., Howland, D., Signer, E., Tobin, A., & Brunner, D. (2009). Systematic behavioral evaluation of Huntington's disease transgenic and knock-in mouse models. *Neurobiol Dis*, *35*, 319–336. doi:10.1016/j.nbd.2009.05.007
- Menalled, L. B., & Chesselet, M.-F. (2002). Mouse models of Huntington's disease. *Trends Pharmacol Sci*, *23*, 32–9.
- Mielcarek, M. (2015). Huntington's disease is a multi-system disorder. *Rare Diseases*, *3*, e1058464.
- Mielcarek, M., & Isalan, M. (2015). A shared mechanism of muscle wasting in cancer and Huntington's disease. *Clin Transl Med*, *4*, 34. doi:10.1186/s40169-015-0076-z
- Mielcarek, M., Smolenski, R. T., & Isalan, M. (2017). Transcriptional Signature of an Altered Purine Metabolism in the Skeletal Muscle of a Huntington's Disease Mouse Model. *Frontiers in Physiology*, *8*, 127.
- Miranda, D. R., Wong, M., Romer, S. H., McKee, C., Garza-Vasquez, G., Medina, A. C., Bahn, V., Steele, A. D., Talmadge, R. J., & Voss, A. A. (2017). Progressive Cl<sup>-</sup> channel defects reveal disrupted skeletal muscle maturation in R6/2 Huntington's mice. *J Gen Physiol*, *149*, 55–74. doi:10.1085/jgp.201611603
- Moffitt, H., McPhail, G. D., Woodman, B., Hobbs, C., & Bates, G. P. (2009). Formation of polyglutamine inclusions in a wide range of non-CNS tissues in the HdhQ150 knock-in mouse model of Huntington's disease. *PLoS One*, *4*, e8025. doi:10.1371/journal.pone.0008025
- Novak, M. J. U., & Tabrizi, S. J. (2010). Huntington's disease. *BMJ*, *340*, c3109–c3109. doi:10.1136/bmj.c3109
- Pereira, L. M., Bastos, C. P., de Souza, J. M., Ribeiro, F. M., & Pereira, G. S. (2014). Estradiol enhances object recognition memory in Swiss female mice by activating hippocampal

- estrogen receptor  $\alpha$ . *Neurobiol Learn Mem*, 114, 1–9. doi:10.1016/j.nlm.2014.04.001
- Piira, A., van Walsem, M. R., Mikalsen, G., Nilsen, K. H., Knutsen, S., & Frich, J. C. (2013). Effects of a one year intensive multidisciplinary rehabilitation program for patients with Huntington's disease: A prospective intervention study. *PLoS Curr*, 5, 1–24. doi:10.1371/currents.hd.9504af71e0d1f87830c25c394be47027
- Prado, V. F., et al. (2006). Mice deficient for the vesicular acetylcholine transporter are myasthenic and have deficits in object and social recognition. *Neuron*, 51, 601–612. doi:10.1016/j.neuron.2006.08.005
- Pratt, S. J. P., Shah, S. B., Ward, C. W., Inacio, M. P., Stains, J. P., & Lovering, R. M. (2013). Effects of *in vivo* injury on the neuromuscular junction in healthy and dystrophic muscles. *J Physiol*, 591, 559–570. doi:10.1113/jphysiol.2012.241679
- Reiner, A., Albin, R. L., Anderson, K. D., D'amato, C. J., Penney, J. B., & Youngt, A. B. (1988). Differential loss of striatal projection neurons in Huntington disease. *Neurobiology*, 85, 5733–5737. doi:10.1073/pnas.85.15.5733
- Reinius, B., Blunder, M., Brett, F. M., Eriksson, A., Patra, K., Jonsson, J., Jazin, E., & Kullander, K. (2015). Conditional targeting of medium spiny neurons in the striatal matrix. *Front Behav Neurosci*, 9, 71. doi:10.3389/fnbeh.2015.00071
- Ribchester, R. R., Thomson, D., Wood, N. I., Hinks, T., Gillingwater, T. H., Wishart, T. M., Court, F. A., & Morton, A. J. (2004). Progressive abnormalities in skeletal muscle and neuromuscular junctions of transgenic mice expressing the Huntington's disease mutation. *Eur J Neurosci*, 20, 3092–3114. doi:10.1111/j.1460-9568.2004.03783.x
- Rice, K. M., Linderman, J. K., Kinnard, R. S., & Blough, E. R. (2005). The Fischer 344/NNiaHSd X Brown Norway/BiNia is a better model of sarcopenia than the Fischer 344/NNiaHSd: A comparative analysis of muscle mass and contractile properties in aging male rat models. *Biogerontology*, 6, 335–343. doi:10.1007/s10522-005-4808-0
- Rodrigues, H. A., Fonseca, M. D. C., Camargo, W. L., Lima, P. M. A., Martinelli, P. M., Naves, L. A., Prado, V. F., Prado, M. A. M., & Guatimosim, C. (2013). Reduced expression of the vesicular acetylcholine transporter and neurotransmitter content affects synaptic vesicle distribution and shape in mouse neuromuscular junction. *PLoS One*, 8, e78342. doi:10.1371/journal.pone.0078342
- Sango, K., McDonald, M. P., Crawley, J. N., Mack, M. L., Tift, C. J., Skop, E., Starr, C. M., Hoffmann, A., Sandhoff, K., Suzuki, K., & Proia, R. L. (1996). Mice lacking both subunits of lysosomal  $\beta$ -hexosaminidase display gangliosidosis and mucopolysaccharidosis. *Nat Genet*, 14, 348–352. doi:10.1038/ng1196-348
- Sartori, R., Schirwis, E., Blaauw, B., Bortolanza, S., Zhao, J., Enzo, E., Stantzou, A., Mouisel, E., Toniolo, L., Ferry, A., Stricker, S., Goldberg, A. L., Dupont, S., Piccolo, S., Amthor, H., & Sandri, M. (2013). BMP signaling controls muscle mass. *Nat Genet*, 45, 1309–1318. doi:10.1038/ng.2772
- Sathasivam, K., Hobbs, C., Mangiarini, L., Mahal, A., Turmaine, M., Doherty, P., Davies, S. W., & Bates, G. P. (1999). Transgenic models of Huntington's disease. *Philos Trans R Soc London B Biol Sci*, 354, 963–969.
- Shirendeb, U. P., Calkins, M. J., Manczak, M., Anekonda, V., Dufour, B., McBride, J. L., Mao, P., & Reddy, P. H. (2012). Mutant huntingtin's interaction with mitochondrial protein Drp1 impairs mitochondrial biogenesis and causes defective axonal transport and synaptic degeneration in Huntington's disease. *Hum Mol Genet*, 21, 406–420. doi:10.1093/hmg/ddr475
- Song, W., Chen, J., Petrilli, A., Liot, G., Klinglmayr, E., Zhou, Y., Poquiz, P., Tjong, J., Pouladi, M. A., Hayden, M. R., Masliah, E., Ellisman, M., Rouiller, I., Schwarzenbacher, R., Bossy, B., Perkins, G., & Bossy-Wetzel, E. (2011). Mutant huntingtin binds the mitochondrial fission GTPase dynamin-related protein-1 and increases its enzymatic activity. *Nat Med*, 17, 377–382. doi:10.1038/nm.2313
- Strand, A. D., Aragaki, A. K., Shaw, D., Bird, T., Holton, J., Turner, C., Tapscott, S. J., Tabrizi, S. J., Schapira, A. H., Kooperberg, C., & Olson, J. M. (2005). Gene expression in Huntington's disease skeletal muscle: A potential biomarker. *Hum Mol Genet*, 14, 1863–1876. doi:10.1093/hmg/ddi192
- Tellez-Nagel, I., Johnson, A. B., & Terry, R. D. (1974). Studies on brain biopsies of patients with Huntington's chorea. *J Neuropathol Exp Neurol*, 33, 308–332.
- Thaut, M. H., Miltner, R., Lange, H. W., Hurt, C. P., & Hoemberg, V. (1999). Velocity modulation and rhythmic synchronization of gait in Huntington's disease. *Mov Disord*, 14, 808–819.
- Valadão, P. A. C., de Aragão, B. C., Andrade, J. N., Magalhães-Gomes, M. P. S., Foureaux, G., Joviano-Santos, J. V., Nogueira, J. C., Ribeiro, F. M., Tapia, J. C., & Guatimosim, C. (2017). Muscle atrophy is associated with cervical spinal motoneuron loss in BACHD mouse model for Huntington's disease. *Eur J Neurosci*, 45, 785–796. doi:10.1111/ejn.13510
- Valadão, P. A. C., Gomes, M. P., Aragão, B. C., Rodrigues, H. A., Andrade, J. N., Garcias, R., Joviano-Santos, J. V., Luiz, M. A., Camargo, W. L., Naves, L. A., Kushmerick, C., Cavalcante, W. L. G., Galacci, M. G., de Jesus, C. G., Guatimosim, S., & Guatimosim, S. (2018). Neuromuscular synapse degeneration without muscle function loss in the diaphragm of a murine model for Huntington's disease. *Neurochem Int*, 116, 30–42.
- Valdez, G., Tapia, J. C., Kang, H., Clemenson, G. D., Gage, F. H., Lichtman, J. W., & Sanes, J. R. (2010). Attenuation of age-related changes in mouse neuromuscular synapses by caloric restriction and exercise. *Proc Natl Acad Sci*, 107, 14863–14868. doi:10.1073/pnas.1002220107
- Valdez, G., Tapia, J. C., Lichtman, J. W., Fox, M. A., & Sanes, J. R. (2012). Shared resistance to aging and ALS in neuromuscular junctions of specific muscles. *PLoS One*, 7, e34640. doi:10.1371/journal.pone.0034640
- van den Bos, M. A., Geevasinga, N., Higashihara, M., Menon, P., & Vucic, S. (2019). Pathophysiology and diagnosis of ALS: Insights from advances in neurophysiological techniques. *International Journal of Molecular Sciences*, 20, 2818.
- van der Burg, J. M., Björkqvist, M., & Brundin, P. (2009). Beyond the brain: Widespread pathology in Huntington's

- disease. *Lancet Neurol*, 8, 765–774. doi:10.1016/S1474-4422(09)70178-4
- Wable, G. S., Min, J.-Y., Chen, Y.-W., & Aoki, C. (2015). Anxiety is correlated with running in adolescent female mice undergoing activity-based anorexia. *Behav Neurosci*, 129, 170–182. doi:10.1037/bne0000040
- Wheelock, V. L., Tempkin, T., Marder, K., Nance, M., Myers, R. H., Zhao, H., Kayson, E., Orme, C., Shoulson, I., & Huntington Study Group. (2003). Predictors of nursing home placement in Huntington disease. *Neurology*, 60, 998–1001. doi:10.1212/01.wnl.0000052992.58107.67
- Willadt, S., Nash, M., & Slater, C. R. (2016). Age-related fragmentation of the motor endplate is not associated with impaired neuromuscular transmission in the mouse diaphragm. *Sci Rep*, 6, 24849. doi:10.1038/srep24849
- Yang, X. W., & Gray, M. (2011). *Mouse models for validating preclinical candidates for Huntington's disease, neurobiology of Huntington's disease: Applications to drug discovery*. Boca Raton, FL: CRC Press.
- Yang, X. W., Model, P., & Heintz, N. (1997). Homologous recombination based modification in *Escherichia coli* and germline transmission in transgenic mice of a bacterial artificial chromosome. *Nat Biotechnol*, 15, 859–865. doi:10.1038/nbt0997-859
- Yap, F. Y., Bui, J. T., Knuttinen, M. G., Walzer, N. M., Cotler, S. J., Owens, C. A., Berkes, J. L., & Gaba, R. C. (2013). Quantitative morphometric analysis of hepatocellular carcinoma: Development of a programmed algorithm and preliminary application. *Diagn Interv Radiol*, 19, 97–105.
- Yu, X. M., & Hall, Z. W. (1991). Extracellular domains mediating epsilon subunit interactions of muscle acetylcholine receptor. *Nature*, 352, 64–67. doi:10.1038/352064a0
- Zhu, X., Yeadon, J. E., & Burden, S. J. (1994). AML1 is expressed in skeletal muscle and is regulated by innervation. *Mol Cell Biol*, 14, 8051–8057. doi:10.1128/mcb.14.12.8051
- Zielonka, D., Marinus, J., Roos, R. A. C., De Michele, G., Di Donato, S., Putter, H., Marcinkowski, J., Squitieri, F., Bentivoglio, A. R., & Landwehrmeyer, G. B. (2013). The influence of gender on phenotype and disease progression in patients with Huntington's disease. *Parkinsonism Relat Disord*, 19, 192–197. doi:10.1016/j.parkreldis.2012.09.012
- Zielonka, D., Piotrowska, I., Marcinkowski, J. T., & Mielcarek, M. (2014). Skeletal muscle pathology in Huntington's disease. *Frontiers in physiology*, 5, 380.
- Zielonka, D., Ren, M., De Michele, G., Roos, R. A. C., Squitieri, F., Bentivoglio, A. R., Marcinkowski, J. T., & Landwehrmeyer, G. B. (2018). The contribution of gender differences in motor, behavioral and cognitive features to functional capacity, independence and quality of life in patients with Huntington's disease. *Parkinsonism Relat Disord*, 49, 42–47. doi:10.1016/j.parkreldis.2018.01.006
- Zuccato, C., Valenza, M., & Cattaneo, E. (2010). Molecular mechanisms and potential therapeutical targets in Huntington's disease. *Physiol Rev*, 90, 905–981. doi:10.1152/physrev.00041.2009